ISSN 0006-2979, Biochemistry (Moscow), 2011, Vol. 76, No. 13, pp. 1484-1506. © Pleiades Publishing, Ltd., 2011.
Original Russian Text © N. A. Koubassova, A. K. Tsaturyan, 2011, published in Uspekhi Biologicheskoi Khimii, 2011, Vol. 51, pp. 233-282.

REVIEW

Molecular Mechanism of Actin–Myosin Motor in Muscle

N. A. Koubassova* and A. K. Tsaturyan

Institute of Mechanics, Lomonosov Moscow State University, Michurinsky pr. 1, 119192 Moscow, Russia; E-mail: natalia@imec.msu.ru

Received May 31, 2011
Revision received June 21, 2011

Abstract—The interaction of actin and myosin powers striated and smooth muscles and some other types of cell motility. Due to its highly ordered structure, skeletal muscle is a very convenient object for studying the general mechanism of the actin–myosin molecular motor. The history of investigation of the actin–myosin motor is briefly described. Modern concepts and data obtained with different techniques including protein crystallography, electron microscopy, biochemistry, and protein engineering are reviewed. Particular attention is given to X-ray diffraction studies of intact muscles and single muscle fibers with permeabilized membrane as they give insight into structural changes that underlie force generation and work production by the motor. Time-resolved low-angle X-ray diffraction on contracting muscle fibers using modern synchrotron radiation sources is used to follow movement of myosin heads with unique time and spatial resolution under near physiological conditions.

DOI: 10.1134/S0006297911130086

Key words: actin, myosin, muscle, ATPase, structure, X-ray diffraction

The interaction of actin with myosin powers motility of striated and smooth muscle and is the basis for many different kinds of biological motility. Due to its regular organization at all structural levels, skeletal muscle is the most suitable object for investigation of the mechanism of the actin–myosin biological motor. This review presents a brief description of investigations of intramuscular actin–myosin interaction and the present-day data of protein crystallography, electron microscopy, biochemistry, and protein engineering. Special attention is given to X-ray studies of intact muscle and isolated muscle fibers with permeable membrane able to generate active force and perform mechanical work. Such studies carried out on advanced sources of synchrotron radiation make it possible to study the motility of myosin molecular motors under conditions close to physiological with high time and spatial resolution.

The first experimental data on structure of the muscle contractile apparatus were obtained by Hugh Huxley using the X-ray diffraction technique [1]. He used a laboratory source of X-ray radiation and a miniature chamber (a window for the 5 μm ray and 3 cm distance between preparation and detector) and obtained small-angle X-ray diffraction patterns of living muscle at rest and under active contraction. These data combined with those of electron microscopy made it possible to design the first scheme of package of thick and thin filaments in a sarcomere. The development of synchrotron radiation sources and occurrence of high-speed two-dimensional detectors opened new possibilities for structural investigations of actin–myosin motor with unique time [2] and spatial [3] resolution. This method is still attractive for present-day experimenters because, unlike many different high technology methods, it allows structural alterations of muscle proteins directly in a cell to be followed simultaneously with changes in its physical parameters.

STRUCTURE OF SKELETAL MUSCLE. MYOSIN, ACTIN, REGULATORY PROTEINS. THE SLIDING FILAMENT THEORY

A skeletal muscle consists of bundles of cells or fibers packed in parallel (Fig. 1). The characteristic cell diameter is 50-100 μm, and the length varies widely. Each fiber is a single big multinuclear cell in which nuclei are located on the surface, while all the remaining space is occu-

* To whom correspondence should be addressed.

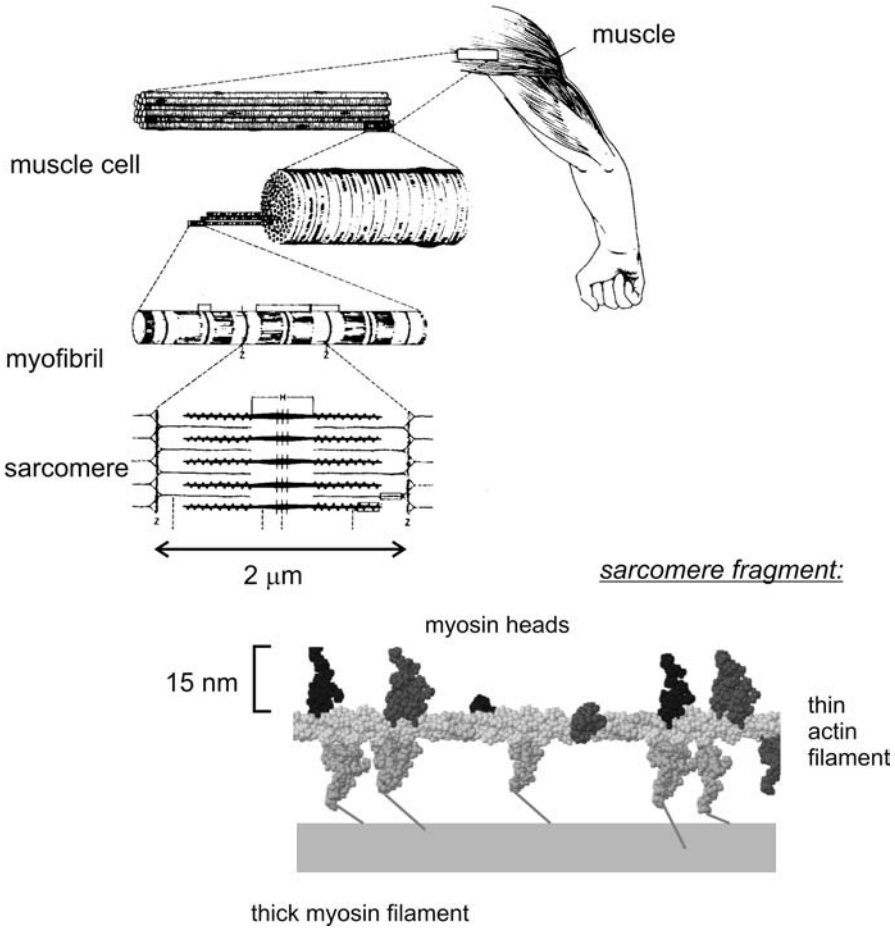

Fig. 1. Scheme of skeletal muscle structure. Characteristic dimensions of a sarcomere and myosin head molecule are shown. Myosin heads belonging to three thick filaments surrounding a thin actin filament are shown in different tones of gray. Actin monomers, accessible for myosin heads, are shown in light gray, and actin monomers bound to molecules of the regulatory protein troponin are shown in lighter gray (regulatory proteins are not shown in the figure).

pied by myofibrils. The diameter of a single myofibril is about 1 μm. Myofibrils consist of equal segments (sarcomeres, derived from the Greek σάρξ – meat and μέρος – portion) separated from each other by Z disks (Fig. 1). In 1674 Anton van Leeuwenhoek used microscope that he constructed and saw the muscle fiber striation caused by regular repeats of sarcomeres. This was a surprising achievement because the sarcomere length is approximately 2.0-2.5 μm.

In the middle of XIX century the German scientist Wilhelm Kuehne isolated the contractile substance of muscle and called it myosin [4]. Later he described it as a substance able to form a contractile clot under certain conditions. At that time no methods for isolation and analysis of pure proteins were available, therefore myosin, partially characterized by Kuehne, really was a mixture of several proteins including actin. At nearly the same time, the description of dark and light zones making striations in skeletal and heart muscle appeared in scientific literature. The lighter sarcomere regions seen in the light microscope were called I (isotropic) zones, while dark zones were called A (anisotropic) zones. Z disks form borders between sarcomeres, while just a very slightly lighter region in the center of A zone was called the H zone (Fig. 2). Russian biochemists showed that extraction of "myosin" from muscle results in disappearance of the A zone high refractive index ([5] and also references in [6]).

The next very important step in investigation of muscle contraction was the discovery by Engelhardt and Lyubimova of the ATPase activity of myosin [7, 8]. They also found that myosin gel was able to change its volume in the presence of ATP. Based on these data, they supposed that ATP cleavage by myosin is the driving force of muscle contraction. This idea is the basis of present-day concepts of the mechanochemical transformation of energy by the actin–myosin motor.

During World War II, in 1942, the Hungarian biochemist Bruno Straub worked in laboratory of Albert Szent-Györgyi at University of Szeged and showed that "myosin" is a mixture of two proteins [9]. The second

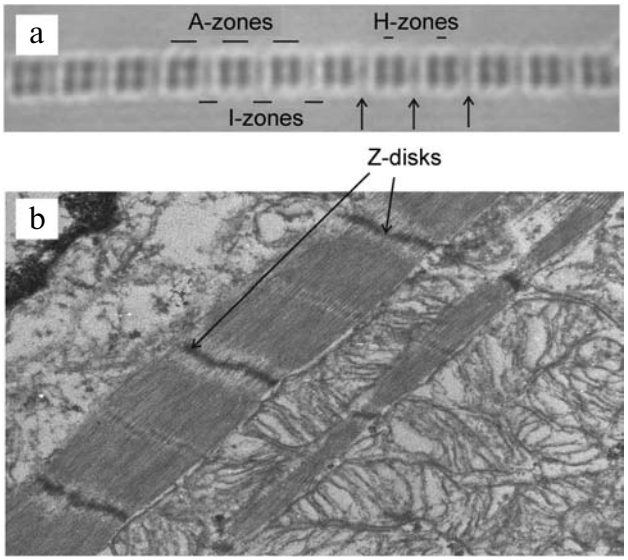

Fig. 2. Contractile apparatus of skeletal muscle. a) The photograph was obtained under a light microscope. Optically distinguished sarcomere zones are shown. b) Electron microphotograph.

protein was called actin due to its ability to activate ATP hydrolysis by myosin. It was shown that actin and myosin dissociate after addition of ATP. Later Szent-Györgyi showed that glycerol-treated muscle fibers containing only the main contractile proteins shorten after addition of ATP [10].

In 1953, Hugh Huxley and Jean Hanson showed using electron microscopy that there are two filament families within sarcomere, thick and thin, but they were very careful in interpreting the results and did not try to combine them with any of the then existing hypotheses on the nature of muscle contraction [11]. In the next year two works appeared independently in *Nature* [12, 13]. The authors used different experimental methods and showed that I zones contain only thin filaments, while A zones contain filaments of both types, and sarcomeres shorten upon contraction so that the length of the A zone does not change and only I zones become shorter (Fig. 3). The authors supposed that the filaments do not change their length upon contraction, but they slide with respect to each other. This hypothesis of sliding filaments was later repeatedly confirmed experimentally and became the basis for present-day concepts on the physics of muscle contraction.

Of course, the term "muscle contraction" is historical and not quite correct. It implies accomplishment by a muscle of mechanical work, i.e. shortening against external force, free active shortening without load, or development of active mechanical tension upon constant length (isometric contraction) in the absence of mechanical work. The muscle is able to lengthen only in response to external forces exceeding the isometric one.

Thin filaments consist mainly of actin protein. Actin is a very widespread and highly conservative protein with molecular mass 42 kDa. Actin monomers (they are often called globular or G-actin) are able to polymerize and form fibrillar F-actin. The polymeric actin filament has helical structure (Figs. 1 and 9) that is often presented as a simple left helix 13/6 (i.e. a complete helix pitch is formed by 13 subunits and contains six full turns). The axial pitch between monomers is about 2.75 nm and the angle of rotation of neighboring monomers is about 167°, i.e. the full period is equal to $13 \times 2.75 \approx 36$ nm [55]. The length of artificial actin filament obtained by G-actin polymerization may reach 20 μm; its length in a sarcomere of the skeletal muscle of warm-blooded animals is about 1 μm. Some other proteins are also present in thin filaments of striated muscle. The most important of them are the regulatory proteins tropomyosin and troponin controlled by Ca^{2+} and providing both activation of muscle contraction and muscle relaxation [14, 15]. Tropomyosin (Tm) was discovered already during the post-war period [16]. Its molecule consists of two mutually twisted α-helices and looks like a long slightly bent helix, approximately complementary to actin helix [17]; the molecular mass of tropomyosin is 65 kDa. Adjacent tropomyosin molecules are joined to each other in the "tail-to-head" manner [18] and form two long rods along the whole actin filament. Troponin is a globular 80-kDa protein discovered in Ebashi's laboratory in the 1960s [19-21]. It consists of three subunits (Tn-I, Tn-C, and Tn-T). Tn-C (calcium binding) exhibits significant affinity to calcium ions, Tn-I (inhibiting) can bind actin, thus fixing the whole troponin–tropomyosin complex on its surface and thus inhibiting both binding of myosin heads

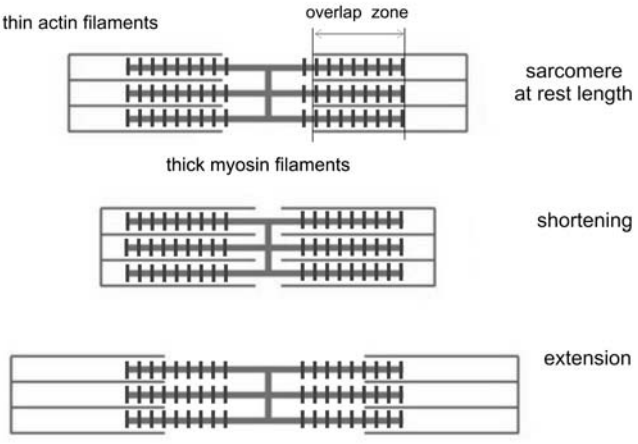

Fig. 3. Illustration of the sliding filament hypothesis. It is seen that when the length of the sarcomere changes, the length of the A zone (the thick filament zone) remains constant and only the length of the I zone (the part of actin filaments not overlapped with myosin) changes. The region including both actin filaments and parts of the head-containing myosin filaments is called the overlap zone.

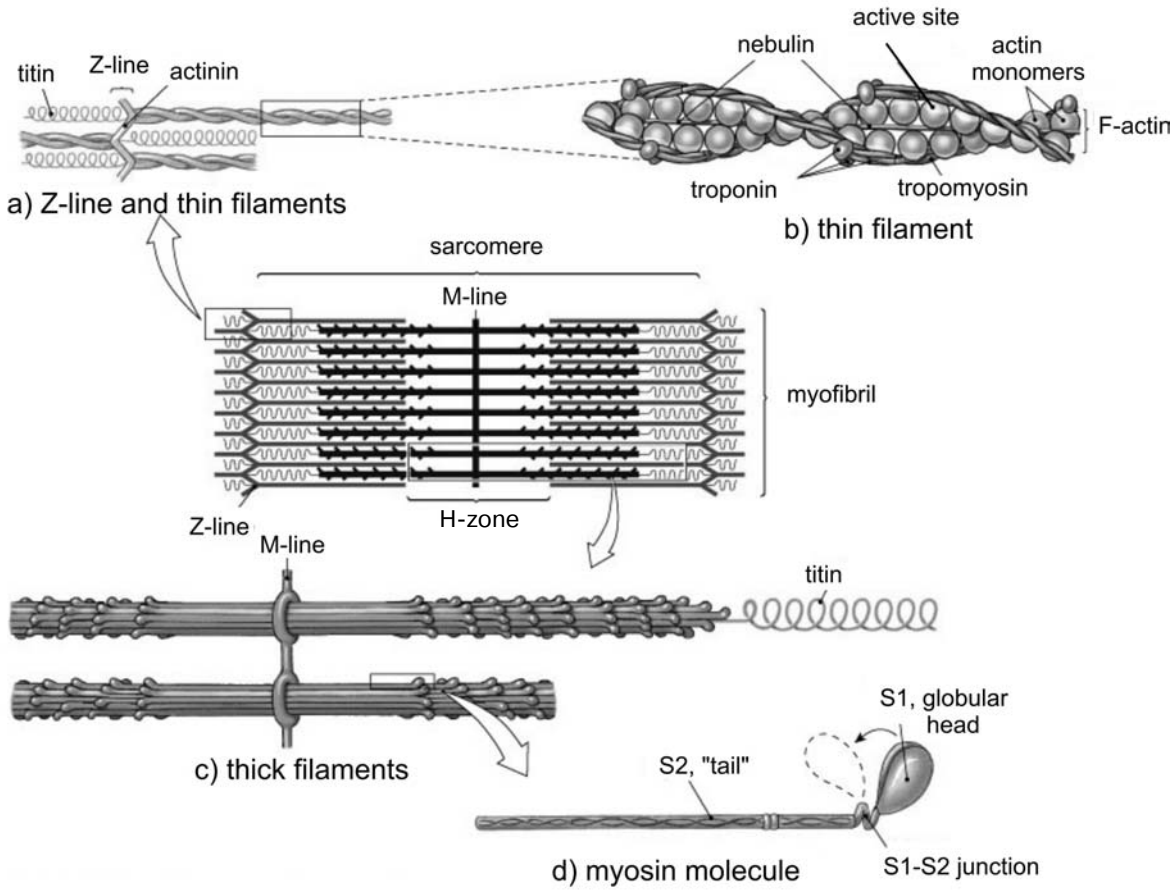

Fig. 4. Scheme of sarcomere structure. Packing of main muscle proteins in thin (a, b) and thick (c, d) filaments is shown. The number of myosin molecules in the thick filament crowns may vary depending on species, in muscle of higher vertebrates being three.

to actin and their ATPase activity, or it itself joins Tn-C, thus weakening contacts of regulatory proteins with actin. Tn-T (tropomyosin-binding) provides association of two other subunits with each other and with tropomyosin. Each troponin complex is bound to one tropomyosin molecule, the axial period of the troponin–tropomyosin complex repeat on the thin filament being 14 pitches of the main actin helix, i.e. 14×2.75 nm ≈ 38.5 nm, a bit higher than the period of the actin helix.

The muscle would not be able to fulfill its function if it constantly existed in "on" condition. The presence of controlled contact "switches" is necessary for efficient work. Calcium ions serve as these "switches". In response to stimulation, intracellular Ca^{2+} concentration increases from 10^{-7} to 10^{-5} M. Depending on localization of Ca^{2+}-binding proteins, the following activation types are distinguished: the myosin one, characteristic of smooth muscle and some mollusk proteins, and actin one, predominant in striated muscle.

The model of actin regulation of striated muscle [22-24] suggests that in response to Ca^{2+} binding to Tn-C [25], troponin turns the bound tropomyosin rod along the surface of actin so that myosin-binding sites are available on actin monomers (Fig. 4). Works of different research groups (for example, [26]) presently deal with investigation of coupling between muscle regulation and mechanics of its contraction.

It is known that the motor protein myosin, forming thick filaments, exhibits high variability [27]. By now, 24 myosin classes have been described and amino acid sequences of over 100 members of this protein superfamily identified [28, 29]. All myosins contain one or two heavy and several light polypeptide chains. The N-terminus of each heavy chain forms a globular myosin head or subfragment 1 (S1) able to bind actin and hydrolyze ATP [30, 31]. ATP hydrolysis results in release of chemical energy that is transformed into mechanical work during the actin–myosin interaction [8].

Myosin head continues to the neck, a long α-helical region of heavy chain, with which light chains are associated. Their number in different types of myosins varies over wide limits. The muscle type II myosin contains two heavy and four light chains. The C-terminal regions of each heavy chain form coiled-coil subfragment 2 (S2) connected via a flexible link to a long rod also coiled-coil region called light meromyosin (LMM). At physiological

ionic strength of the surrounding solution, rod regions of myosin molecules aggregate and form myosin filaments (Fig. 4). In skeletal muscle these filaments have helical symmetry and constitute a three-strand right helix with period of about 43 nm and axial distance between crowns of protruding myosin heads ~14.3 nm. Long superhelical parts of myosin molecules (LMM) form the backbone of the 15-nm thick myosin filament. In addition to the main protein of thick filament, myosin, there are also different proteins like titin, myosin binding protein C, MyBP-C, etc. [32, 33].

CROSS-BRIDGE MODEL OF MUSCLE CONTRACTION, LEVER ARM HYPOTHESIS

The first molecular theories describing the mechanism of muscle contraction appeared in the 1930s, but none of them was correct. The basis of present-day concepts is the above-described hypothesis of sliding filaments [12, 13]. In these works there was a question concerning the force that makes filaments slide, and it was supposed that some structures joining thin and thick filaments are responsible for this action. Soon it was shown using electron microscopy that there are protrusions of myosin filaments forming cross-bridges with actin [34, 35], and it was shown later that just myosin heads, forming these bridge, exhibit ATPase activity. Two positions of cross-bridges were found in the flight muscle of insects: perpendicular to actin filaments and inclined at approximately 45° [36].

Structural and biochemical experimental data available at the beginning of the 1970s were combined in the scheme of Lymn and Taylor (Fig. 5a [37, 38]).

According to this scheme, myosin head together with ATP or its hydrolysis products ADP and inorganic phosphate (P_i) bind actin in the pre-force-generating state (in Fig. 5 it is shown at the right angle, state 4). Hydrolysis

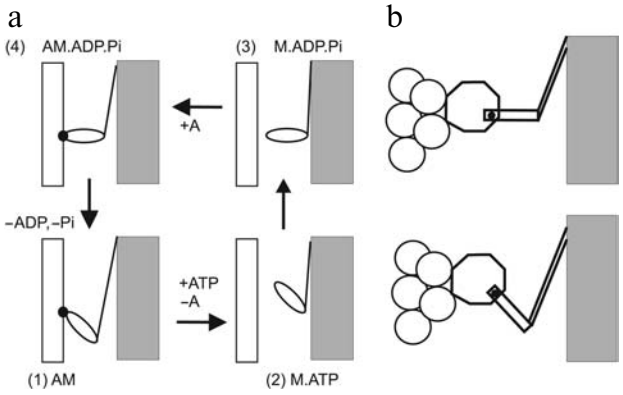

Fig. 5. a) Lymn–Taylor scheme of cross-bridge working cycle. b) Hypothetical conformational changes in myosin head during working step [42, 43].

itself or ATP cleavage to ADP and P_i takes place in the detached state. In the absence of actin, the rate of ATP hydrolysis by myosin does not exceed 0.05 sec^{-1} and is limited by release of P_i [39]. If myosin molecules are packed in a thick filament, then in conditions, corresponding to relaxed state myosin heads form an ordered structure on the filament surface [40]. In this case the rate of ATP hydrolysis becomes additionally 10 times lower [41]. This low rate of ATP hydrolysis by myosin explains why the relaxed muscle consumes little energy.

The binding of S1 to actin speeds up phosphate release, results in alteration of S1 shape and enables the heads to perform work (Fig. 5a, state 1). This, in turn, stimulates ADP release from the S1 active center, after which binding of a new ATP molecule causes dissociation of S1 from actin [37, 38]. In the absence of ATP the head binds actin in state 1 corresponding to the end of working cycle; this state is called *rigor* (from *rigor mortis*). Since there is an excess of ATP in a living muscle cell, myosin head resides in this state for a short time. One ATP molecule is spent for one working cycle of the cross-bridge.

Experiments allowing estimation of physical characteristics of molecular motor were carried out approximately at the same time [44]. The researchers used rapid (~1 msec) changes in the length of contracting single intact fiber from frog muscle and registered tension developed by the fiber in response to its extension or shortening. This approach suggests the use of disturbance of equilibrium conditions, in this case – of microscopic mechanical events in separate bridges, to synchronize these events to the macroscopically measurable response of the whole fiber tension and to interpret this response in terms of the averaged cross-bridge reactions. The authors believed that the cross-bridge joined to the thick filament by an elastic element (supposedly the S2 element) rotates on the thin filament surface over a series of discrete states without changing the shape, and that the rigidity of both thick and thin filaments much exceeds that of cross-bridges; keeping all this in mind, the authors built a model that quite satisfactorily described results of mechanical experiments. According to the authors' concepts, the cross-bridge "working step", i.e. the distance covered by the head upon cleavage of a single ATP molecule, is 8-10 nm.

The hypothesis that the force development is the result of tilt of the cross-bridges was confirmed in X-ray diffraction experiments. The brightest meridional reflection M3 on the X-ray diffraction pattern of contractile muscle, corresponding to an axial period of ~14.5 nm, is caused by the repeat of bridge crowns along the rod of the thick filament (Fig. 9). If an average cross-bridge tilts upon contraction in accordance with the Lymn–Taylor scheme, this reflection would be weaker. All attempts to register similar changes using laboratory sources of radiation were not successful because reliable data can be obtained on such sources after muscle exposure to X-rays for many hours, so that muscle injury appeared great

before the reliable measurement of reflection intensity became possible. The first centers using synchrotron radiation for investigation of biological objects were built in Hamburg (DESY [45, 46]). Key experiments were carried out in the 1980s. It was shown that the change in the 14.5 nm reflection intensity takes place on the same millisecond time scale as the tension changes [47]. If the contractile muscle undergoes rapid shortening like in experiments of Huxley and Simmons [44], then the intensity of the M3 meridional reflection decreases. If the specimen quickly (during 1-2 msec) returns to its initial length, the reflection intensity also returns to the initial level. However, if the specimen length was not restored and kept constant after shortening, then the reflection intensity was also restored, although much more slowly [48]. As soon as all used methods were improved, these experiments were repeated on single intact frog muscle fiber at the synchrotron radiation source SRS with submillisecond time resolution (Daresbury Laboratory, GB) [49]. Experimental recording of cross-bridge movements simultaneously with changes in tension provided powerful support of the tilting cross-bridge hypothesis.

In the second half of 1980s *in vitro* motility systems were created in which proteins actin and myosin, isolated from muscle, moved relative each other *in vitro* in the presence of ATP [50-52]. Thus, it was finally proved that ATP, actin, and myosin, or more exactly S1, are able to provide active mechanical motility in the absence of supramolecular organization and other substances.

Remarkable experiments were carried out by Hugh Huxley et al. They registered changes at the second actin layer line upon activation of the whole muscle. It appeared that the increase of intensity at this line over sufficiently large reciprocal radii happens immediately after the beginning of activation and leaves tension development behind. Such intensity increase could be caused only by the thin filament proteins, namely by the tropomyosin turn along the actin surface which intensifies four-folded filament symmetry. This was an obvious confirmation of the mechanism of steric regulation of the thin filaments [53].

In 1990, protein crystallography was used to obtain the first atomic structure of actin monomer and to propose a model structure of F-actin [54, 55], while the atomic structure of S1 of chicken muscle myosin was determined in 1993 [56]. Later different actin and S1 structures were also obtained. The latest actin model that can be considered as really atomic was obtained recently [57]. It appeared that conformation of actin monomers noticeably changes upon polymerization. This explains why only actin filaments rather than globular actin are able to bind myosin and maintain its motility.

The myosin head or the myosin proteolytic fragment S1 contains a heavy chain (95 kDa) and two associated light chains (~15-20 kDa each). It retains the whole enzymic activity of myosin and is the minimal fragment that retains motor activity of the whole molecule. Further proteolysis divides the S1 heavy chain to three fragments named after their molecular mass values 25 kDa N-terminal fragment, 50 kDa central fragment, and 20 kDa C-terminal fragment. The first crystallographic structure of S1 was obtained at high salt concentration and in the absence of bound nucleotide [56], its heavy chain contains 843 amino acids (PDB code 2MYS).

It appeared that myosin head resembles in shape the head of a small beast with slightly open jaws (Fig. 6). A long neck is formed by the heavy chain α-helical region and associated light chains, one of which is called essential, and the other regulatory. The neck as a lever increases small changes in converter domain to significant changes; in terms of protein, these are transfers of C terminus where the head is connected to S2 and then to the thick filament. In fact, the motor head region consists of several domains involved in binding of actin and ATP (and after hydrolysis – to its hydrolysis products P_i and ADP). The cleft divides the central 50 kDa domain to two subdomains, upper and lower, and both of them are involved in actin binding. The ATP binding site or "pocket" is local-

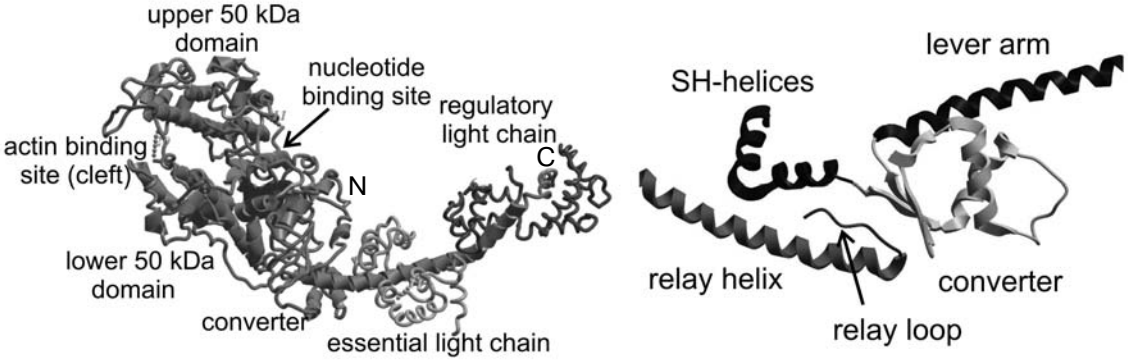

Fig. 6. Structure of myosin head (S1) according to [56]. A general view is shown on the left and the main structure–functional elements are designated; the region of catalytic domain contact with lever arm and some of their details are shown at high magnification on the right: relay helix, relay loop, and converter.

ized between the upper "jaw" (upper subdomain) and N-terminal region of S1 and is situated near a 7-strand β sheet. This sheet serves as a "frame" to which the main motor details are fixed. The lower "jaw" is also joined to the ATPase active center via "switch-2". All these details can move relative to each other and their correct coordinated movement provides the motor functioning.

Soon after first S1 structure was determined, rather quickly several other structures of different types of myosin heads in different configurations were obtained [58-67]. Biochemists offered enormous help to crystallographers when they discovered the way to express short-fragment myosin motor domain [68]. Although obtaining the atomic structure of the complete S1 is a heroic problem, the shortened S1 (without the long "lever" or its part) are crystallized rather easily. It appeared that S1 of myosin II from scallop muscle crystallizes better than S1 of striated muscle of vertebrates, and their crystal structures very much resembled each other [69].

It appeared that most determined S1 structures could be divided into two classes depending on the content of their active center. These two classes differ by the orientation of the converter domain by approximately 60°. Since the long neck of S1 is strongly bound to the converter, upon its turn the neck turns as a lever relative to the catalytic (and actin-binding) S1 domain. Such rotation, in turn, is equivalent to the axial movement of the S1 C-terminal region by 8-10 nm relative to its actin-binding site.

It was shown experimentally that the rate of unloaded movement of the actin filaments along the myosin-covered surface linearly depends on the length of its α-helical neck, which can be changed using gene engineering techniques [70].

These results lead to the proposal of the "lever arm" hypothesis ([42, 43], Fig. 5b). According to this hypothesis, the "lever arm" tilt is the process that results in relative sliding of the thick and thin filaments, while bound catalytic domain S1 does not change its position on actin. Since this hypothesis was formulated on the basis of investigation of S1 crystal structure in the absence of actin, it remains unclear whether in reality all changes in actin–myosin complex, which provide tension development or filament sliding, are limited only by rearrangement within S1 and do not include changes in the zone of its contact with actin. To answer this question, it is necessary to have data on structural changes of the actin–myosin complex in functioning system, able to develop active force and sliding.

Myosin V is an intracellular transport protein. It delivers vesicles via long actin bundles from the cell center to its periphery. Like myosin II, it is two-headed, but its neck is much longer, and therefore it is able to move by big steps equal to a full 36 nm period of actin helix. Unlike myosin II, myosin V is a processive protein, i.e. its single molecule is able to move along actin, so at any moment at least one of its heads is bound to actin and therefore it is able to transfer the load alone for a significant distance along the filament. From a biochemical point of view, this means that even after being bound to ATP or ADP and phosphate, S1 of myosin V is strongly bound to actin. In the structure of shortened S1 of myosin V without nucleotide, obtained by X-ray crystallography, the cleft between upper and lower jaws of the central domain is closed [64].

Comparison of the new S1 structure with the earlier obtained one has shown that closing the cleft also coincides with the movement of switch-1, which opens the nucleotide-binding pocket and bending of the β-sheet [64]. Very similar changes in the position of switch-1 and in β-sheet are seen in structure of S1 of the *Dictyostelium* myosin II in the absence of nucleotide [71]. As is shown in experiments [72], unlike myosin V, the switch-1 opening in myosin II in the absence of nucleotide does not result in cleft closure. S1 binding to actin is necessary to achieve this. Therefore, just structures with closed cleft correspond to the myosin state firmly bound to actin and can serve as a model of the rigor state, and all structures with separated upper and lower jaws correspond to the myosin weakly binding actin. Later S1 structures of myosin II were obtained for myosin preparations isolated from some sea animals in which switch-1 was open in the absence of nucleotide and the cleft was closed, also not so tightly as in myosin V [67]. Now structural states of S1 with low affinity to actin are classified as pre-force-generating and post-rigorous, depending on lever position. The first obtained structure of myosin II head from chicken muscle [56] belongs just to the post-rigor class.

It is interesting to trace the relationships of structural data with results of biochemical experiments carried out with S1, actin, and ATP in solution. This is the subject of a large review [69], but here we shall emphasize only key points.

The tightness of the myosin head binding to actin is maximal if the ATPase pocket is empty or contains only ADP. The constant of equilibrium between free and actin bound S1 is below 0.1 μM. Under conditions of intramuscular ATP exhaustion, all myosin heads firmly bind actin and muscle becomes very rigid, i.e. muscle goes to the rigor state. This happens because for tight actin binding the upper and lower jaws should approach and close the cleft between them (Fig. 7). Only in this case the actin-binding site of the head becomes complementary to the corresponding actin surface and is capable of tight binding to the latter (Fig. 7). Upon closing of the cleft, the upper jaw as a whole rotates relative the rest of the catalytic domain and opens the ATPase pocket. Thus, the active and actin-binding S1 centers function in conformity, although they are localized at a distance of 3-4 nm from each other. If ATP or both its hydrolysis products ADP and P_i are present in the head active center, then the tightness of their binding to actin decreases almost 1000-

fold. This happens because ATP binding results in pocket closure and, correspondingly, in cleft opening. During the time when the active center remains closed, the actin-binding cleft is open independently of hydrolysis. In this case S1 can easily dissociate from actin and then bind another monomer. It is necessary for successful hydrolysis that the pocket of the active center should be completely closed because only in this case establishment of numerous bonds is possible between atoms of protein amino acids, Mg, and ATP that weaken binding between γ phosphate and the remaining part of the ATP. Without this, a water molecule is not able to cleave ATP. There is dynamic equilibrium between the active center open and closed states [73, 74]. It is strongly temperature dependent: temperature increase stimulates closing of the nucleotide "pocket".

There is certain competition between S1 binding to nucleotide and actin. The binding constant of ATP or ADP to S1 significantly decreases if S1 is tightly bound to actin. This is evidently explained by the fact that tight binding to actin is accompanied by a rotation of the upper "jaw". Such rotation results not only in the closure of the cleft but also in opening of the nucleotide "pocket" (Fig. 7), which makes the nucleotide binding weaker. In contrast, binding of ATP or its analogs to S1 makes weaker its affinity to actin, because it stimulates closing the nucleotide pocket and opening the cleft at the actin-binding surface of S1.

Note, at first sight a paradoxical fact: ATP hydrolysis *per se* in S1 is easily reversible – the equilibrium constant of this reaction is about 10, i.e. one ATP molecule is synthesized *de novo* from ADP and P_i for 10 hydrolyzed ATP molecules, which corresponds to the difference of free energies altogether in $k_BT\ln(10) \approx 10^{-20}$ J, where k_B is Boltzmann constant and T is absolute temperature. Free energy of ATP hydrolysis is ten times higher, about 10^{-19} J. For what is the rest of the energy spent? It is accumulated within the myosin head – the motor "is charged" and is ready "to fire" – to carry out mechanical work upon interaction with actin. Translocations of separate S1 details upon ATP binding are small. However, internal stress values within the S1 molecule are, evidently, rather high. For example, they result in untwisting of rigid β sheet [69].

Now we shall consider the motor work cycle beginning from the stage when the head bound and hydrolyzed ATP, i.e. it is completely "charged" and ready to work. If actin is inaccessible, then the ATP hydrolysis products remain for a long time in the active center, until, due to large-scale and therefore rare fluctuation, the ATPase pocket does not open itself and P_i and then ADP too become able to leave the active center. S1 is able to bind a new ATP molecule only after release of the hydrolysis products. Owing to such slow discharge of products, the S1 head in relaxed muscle cleaves only two ATP molecules per minute, and the fuel expense during rest is very low. In condition of active contraction, phosphate release

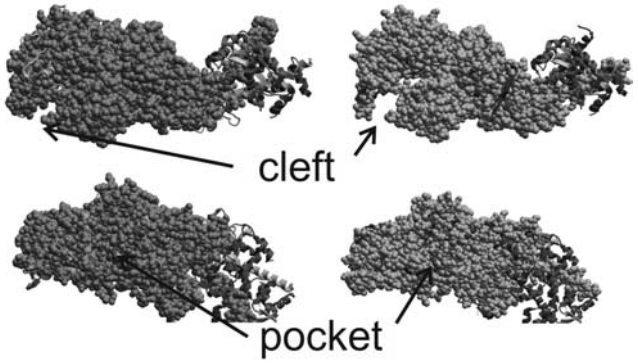

Fig. 7. S1 myosin V structures without nucleotide (left, PDB code 1W8J) and in the presence of ADP and inorganic phosphate analog BeF (right, PDB code 1W7J). Upper and lower pictures were obtained by turning by 90°. To visualize the nucleotide pocket of free S1, the ATP molecule was deliberately inserted into it. The figure was obtained using the ICM (Molsoft, USA) program.

is sharply accelerated. The interaction of the head with actin passes over several stages. In the first stage the head weakly binds actin, mainly due to electrostatic interaction of negatively charged groups on the actin surface with positively charged groups in the disordered loop 2 between the upper and lower jaws of S1. In the second stage, the jaws join and the weak bond with actin is transformed to the tight one. It is not known exactly how and why the presence of actin stimulates closing of the S1 cleft, because all atomic structures of myosin heads were obtained in the absence of actin. As was said above, cleft closure is accompanied by a rotation of the upper jaw and partial opening the ATPase pocket.

The next stage is associated with release of stored energy and its transformation into mechanical work. Formation of S1 tight complex with actin and closing the cleft also makes easier movement of switch-1 that binds the lower "jaw" with the ATPase pocket. Small, only 0.2-nm switch movements stimulate large-scale rearrangement of the whole myosin head. Switch movement pass to the lower jaw of S1 and causes there a set of conformational changes. The opening of switch-1 results in twisting of one, partially untwisted turn of the so-called "relay" α-helix extended from the lower jaw actin-binding site to the "lever arm" region (Fig. 6). This results in a rotation of the relay-loop at the end of relay-helix and its shift relative to so-called SH helix. After these changes in lower part of S1 low 50-kDa domain, being in tight contact with the rigid lever arm domain called converter, the latter turns by 60-65°, thus "switching over" to an energetically more advantageous position. Since the lever length is 8 nm, such turn causes the shift of its terminus by 10 nm, a distance that many times exceeds the switch motion. Just the displacement of the distal part of the lever arm along the actin axis is an elementary "step" of the myosin motor.

When, after the turn of the upper jaw and the switch-1 coming into action, thus causing a turn of the lever, the ATPase pocket of S1 completely opens, and the hydrolysis products easily leave it and free the place for a new ATP molecule. Therefore, actin binding accelerates the cycle of ATP hydrolysis by a single myosin head at up to 40 molecules per second, which is at least 100 times more rapidly than in the absence of actin [75]. ATP binding and pocket closing, in turn, result in cleft opening and weakening the binding of the head to actin. Now it is easily detached from the latter. Binding of a new ATP molecule results in pocket closing. When it is completely closed, it draws the switch in and the lever arm returns to initial position. Now the motor is "charged" *de novo* and is ready for a new cycle of work with involvement of another actin monomer.

Note again that the above-described scheme of myosin motor work is based on comparison of different S1 crystal structures obtained in the absence of actin. Therefore it is still not clear how its interaction with actin as well as forces developed upon actin–myosin interaction and translocations in organized system within sarcomere influence the alteration of S1 shape and what changes in the actin–myosin complex really result in carrying out mechanical work.

X-RAY DIFFRACTION PATTERN OF MUSCLE

Myofibrils in skeletal muscle are so well arranged that the package of contractile proteins in a sarcomere is close to crystalline. Actin, myosin, and other proteins of thick and thin filaments generate a rich set of equatorial and meridional reflections and layer lines on diffraction diagrams. In the first works by H. E. Huxley on diffraction of muscle, these reflections were successfully used for obtaining information on muscle structure in different physiological and biochemical conditions [1, 76].

The scheme of the X-ray diffraction experiment is shown in Fig. 8. The specimen is placed in the experimental set up. The incoming beam of monochromatic X-ray radiation scatters on the specimen, and scattered radiation is registered by a two-dimensional detector. Since muscle exhibits low scattering power for X-rays and does not form a really crystalline structure, all registered reflections are localized within the small angle regions and therefore a flat detector can be used. Specimens in experiments are set vertically or horizontally. It is more convenient to work with horizontally set preparation, but vertical position provides better spatial resolution along the meridian because the synchrotron beam is better collimated in vertical direction than in the horizontal.

Contemporary sources of synchrotron radiation generate a beam of monochromatic X-rays up to intensity of $5 \cdot 10^{13}$ photon/sec with a size of 0.2-0.3 mm that only slightly exceeds the muscle fiber diameter. This makes it possible to obtain X-ray diffraction movie of a single cell with resolution 1000 frames/sec and to achieve the record time resolution of 0.02 msec for the brightest M3 reflection [2]. Fast perturbations can be used to synchronize movements of separate motor molecules. Such effects can

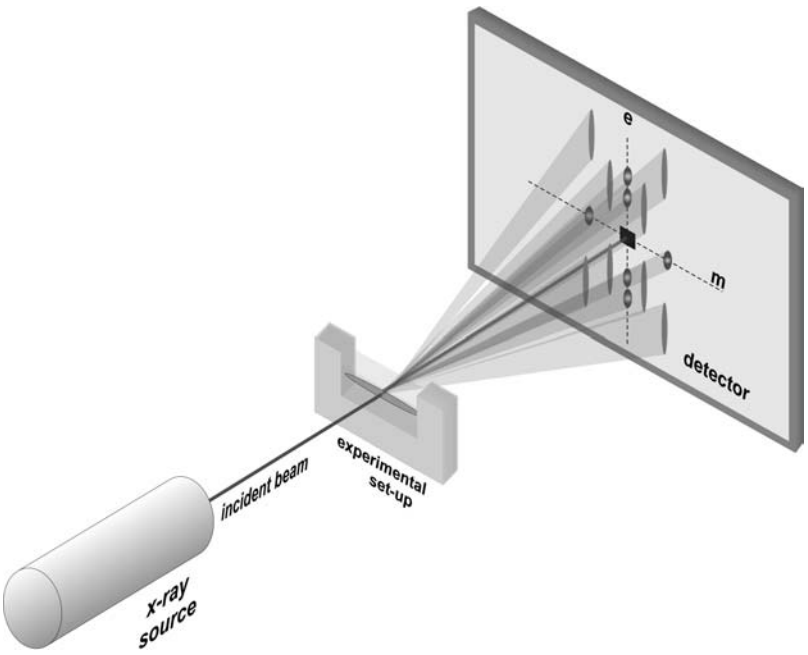

Fig. 8. Scheme of X-ray diffraction experiment. Equatorial and meridional axes of detector are marked by letters "e" and "m", respectively.

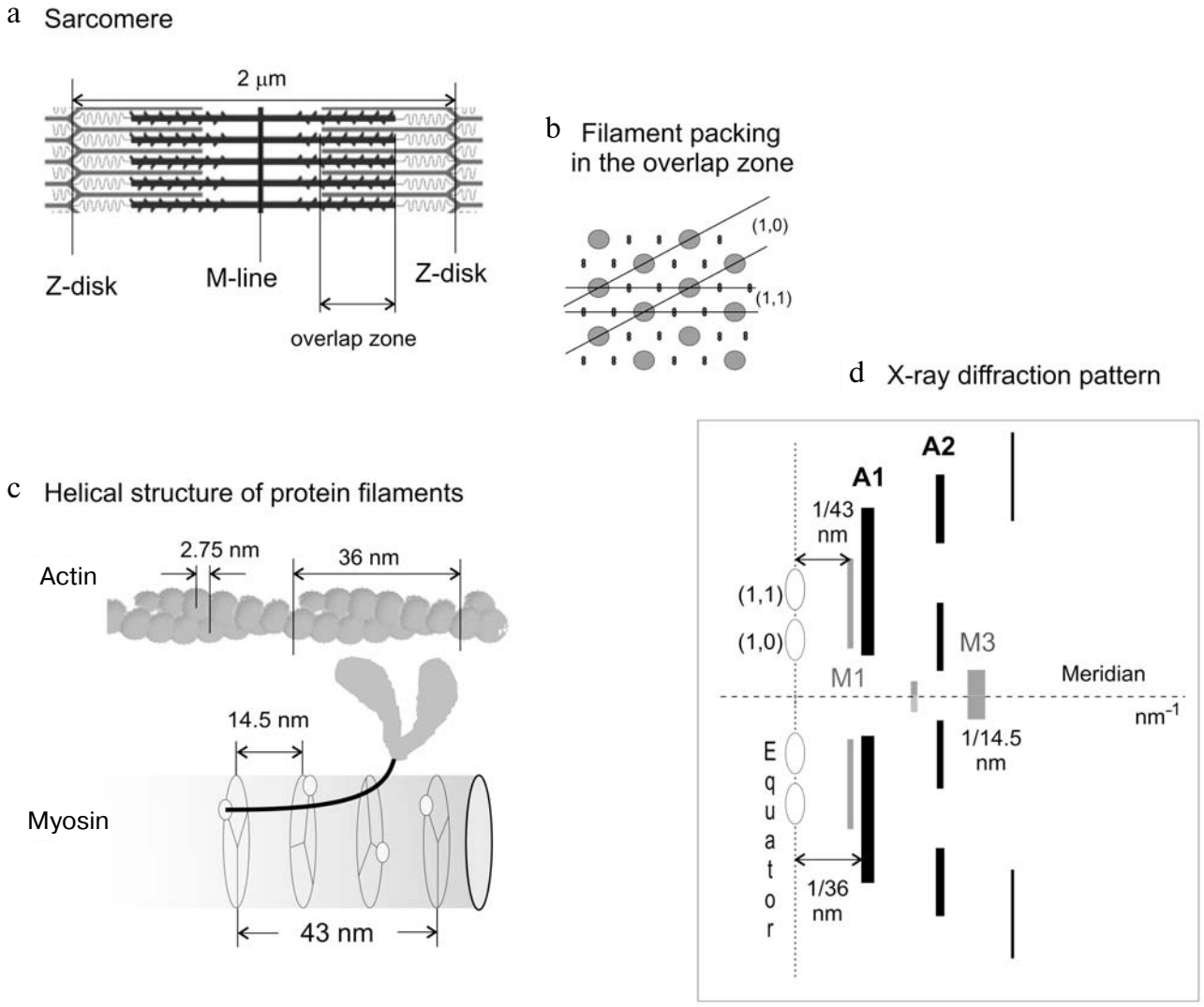

Fig. 9. Periodic protein structures of sarcomere and corresponding reflections on the skeletal muscle X-ray diffraction pattern. Parameters of helices of actin and myosin filaments are shown in panel (c). Helix pitch (axial distance between neighboring monomers) of actin is ~2.75 nm and its period (complete repeat) is ~36 nm; the myosin helix pitch is 14.5 nm, its period is ~43 nm.

include rapid stepwise changes of the length of contracting muscle or of a single fiber [49], sub-millisecond jump in temperature [77, 78], photolytic ATP release from its non-hydrolyzable analog in response to a flash of the ultraviolet laser light [79, 80], or pressure jump [81].

The brightest reflections are seen on equator, the detector axis perpendicular to that of the fiber. Reflections on the meridian, the detector axis parallel to that of fiber are noticeably weaker. The layer lines are reflections in the form of lines parallel to the equator, in general are even less bright than the meridional reflections. The correspondence between the sarcomere protein structures and X-ray diffraction pattern is shown schematically in Fig. 9. Here and below we shall designate as structure period its value in physical space having dimension in nm, while reflection spacing or coordinate will correspond to its value in the reciprocal space, i.e. with dimension nm^{-1}. As period increases, spacing of corresponding reflection decreases.

Experimental X-ray patterns of single fiber of rabbit skeletal muscle in rigor and in isometric contraction at 30°C are shown in Fig. 10.

Equatorial Reflections

In a sarcomere, in the overlapping zone, thick and thin filaments form a hexagonal lattice in which myosin filaments are localized at the lattice points, while actin filaments are in triangle points (Fig. 9b [82]). Diffraction on such a lattice gives a specific set of equatorial reflections (Fig. 9d). Since the orientation of the lattice in dif-

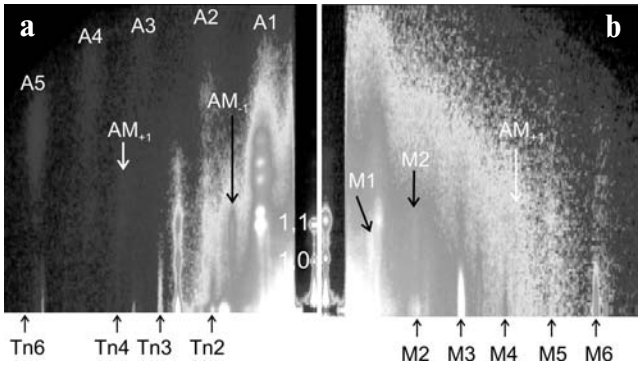

Fig. 10. X-Ray diffraction pattern of a single fiber of rabbit skeletal muscle in rigor (a) and in active contraction at 30°C (b). For each state only one of four symmetrical quadrants (0.155 nm^{-1} × 0.155 nm^{-1} in reciprocal space) is shown, the equator position being vertical. Two ~3.5 mm segments of permeabilized muscle fiber were used, exposure for 400 msec in each state, camera length 4.2 m; intensity is shown in logarithmic scale to make visible both weak and bright reflections, the lighter is the point color, the higher is the intensity in it. The brightest reflections are labelled. An attenuator was placed on the detector along the equator to prevent detector saturation.

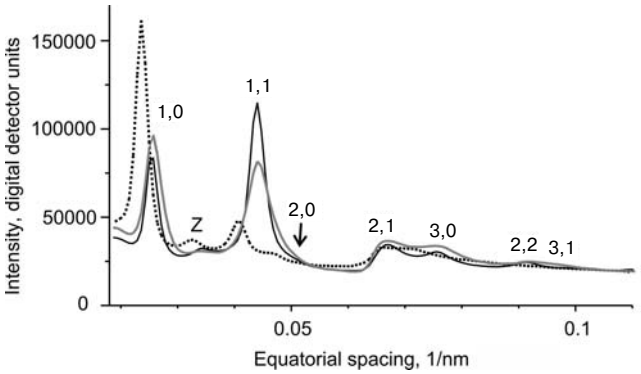

Fig. 11. Diffraction of muscle in the equatorial plane. The equatorial intensity profile on X-ray photograph of a single permeabilized fiber of flounder fin muscle in relaxed state (dotted line), in rigor (black), and during isometric contraction at 5°C (gray). Data were obtained on station ID02 of the European Synchrotron Radiation Facility (ESRF). Exposure time in each state is 100 msec, wavelength is 0.1 nm, the length of chamber is 2.5 m. An attenuator placed along the equator lowered intensity in the region of reciprocal axial coordinates below 0.064 nm^{-1} to prevent detector saturation. The main reflections are labeled. Here and in Figs. 12 and 13, arbitrary units mean units of CCD detector.

ferent myofibrils is random relative to the incoming beam, the X-ray diffraction pattern of the muscle shows the square of Fourier transform of protein filament electron densities averaged over all possible azimuth angles. Any equatorial reflection contains contribution of only those sarcomere regions for which the angle between the corresponding plane (h,k) and incoming beam is equal to the Bragg angle for a given reflection.

Two brightest equatorial reflections 1,0 and 1,1 correspond to diffraction on the planes shown in Fig. 9. The period of these reflections is equal to $\sqrt{3}d/2$ for (1,0) and $d/2$ for (1,1), where d is the distance between two neighboring thick filaments within the sarcomere. Changes of absolute values and ratios of intensities of these reflections $I_{1,0}$ and $I_{1,1}$ were noticed in comparison of the relaxed muscle X-ray patterns with those of muscle in rigor condition ([83], Fig. 11). In rigor $I_{1,1}$ increases, while $I_{1,0}$ decreases. Qualitatively this can be explained by movements of myosin heads, in relaxed muscle concentrated near the myosin filament surfaces or in planes (1,0), towards actin filaments localized in planes (1,1) [83]. In active contraction, $I_{1,0}$ and $I_{1,1}$ acquire intermediate values between those that are achieved in rigor and at rest (Fig. 11 [84]).

The ratio $I_{1,1}/I_{1,0}$ was used for estimation of the fraction of myosin heads in active contraction [84, 85]. This approach is still used [86], especially for studies of heart muscle [87]. However, intensity distribution along the equator depends not only on the number of attached heads, but on some other parameters as well. In particular, this distribution is much influenced by the extent of actin–myosin lattice ordering [88].

In non-overlapping sarcomere zones (I zones), thin filaments form a different rectangular lattice caused by geometry of their incorporation into the Z line [82]. This rectangular lattice is seen on the equator as the Z reflection localized between reflections 1,0 and 1,1 (Fig. 11).

The equatorial reflection intensities are also influenced by distribution of detached heads around thick filaments. It was shown that in relaxed mammalian muscle increasing temperature from 5 to 20°C stimulates transition of detached myosin heads from disordered state into helical package on the backbone of the thick filament [89]. This transition is also accompanied by decrease in $I_{1,1}/I_{1,0}$ ratio [89, 90] and increased disorder of actin filaments observed on electron microphotographs [91, 92].

It is also known that small changes in lattice size cause significant changes in equatorial reflections [88]. In the case of the skinned muscle fiber transition from relaxed state to rigor the lattice shrinks. Upon increasing ionic strength the decrease in lattice spacing can reach 10% (Fig. 11). In intact muscle fiber development of contraction does not result in any significant lattice shrinkage [93]. A slight reduction of lattice spacing takes place when the fiber develops active tension in the presence of ATP and Ca^{2+} (Fig. 11). This is probably due to the radial component of the active strength of cross-bridges [94]. An intact fiber in tetanus upon feedback of sarcomere length also shrinks but rather little, about 2% [93]. In heart muscle changes in lattice spacing due to changes in sarcomere length and activation extent may explain the known Frank–Starling law [95, 96].

Meridional Reflections

Meridional reflections on the X-ray diffraction pattern indicate structures exhibiting periodicity along the fiber axis. Meridional distributions of intensity on a low-angle X-ray pattern of rabbit skeletal muscle are shown in Fig. 12.

Meridional reflections of thin filaments. The main actin meridional reflection corresponds to the distance between two adjacent monomers, its position in reciprocal space being ~$(2.75\ \text{nm})^{-1}$ (Fig. 9). We call this reflection A13 in accordance with the simplest model of actin helix 13/6 in which 13 monomers fall within six full turns of left-hand helix. Binding of myosin heads to actin in rigor or during active contraction results in increase in A13 intensity (Fig. 12b) due to efficient increase in electron density of the actin helix.

Changes in this reflection position were used for determination of the thin filament axial extension upon increase in tension, Ca^{2+}-activation, and upon myosin head binding to actin filament. In X-ray diffraction experiments, the compliance of actin filaments was estimated as 0.2-0.3%/T_0, where T_0 is isometric tension equal to 200-300 kPa for the whole frog *m. sartorius* at 10°C [97, 98]. Soon it was shown that activation causes shortening the actin filament, and estimations of actin extensibility increased to 0.6%/T_0 [99, 100]. We have shown that strong binding of myosin heads to actin without development of high tension results in 0.2% elongation of thin filaments [101]. With account of these results, the value of thin filament compliance obtained in our previous mechanical experiment [102] now agrees with X-ray diffraction data.

In addition to actin meridional reflections (A13 and its higher orders) in thin filaments, there is always an additional series of meridional reflections caused by repeated axial structure of the thin filament regulatory proteins. Troponin and tropomyosin have an axial period of ~38.5 nm, which exceeds the period of the actin helix; it is about 14 times longer than the pitch of the actin helix. The contribution of troponin to meridional reflections is evidently significantly higher than the contribution of tropomyosin; therefore, these reflections are called troponin Tn1, Tn2, and Tn3 (Fig. 10). Intensities of these reflections also change upon change of muscle condition (Fig. 12a [103]).

Meridional reflections of thick filaments. Thick filament reflections are called myosin reflections, although they are in part due to diffraction on other thick filament proteins. Their period is approximately 43 nm, i.e. position M1 ≈ $(43\ \text{nm})^{-1}$, of next maximum M2 – 2/43 = $(21.5\ \text{nm})^{-1}$, 3/43 nm = $(14.33\ \text{nm})^{-1}$ for M3, etc. (Fig.

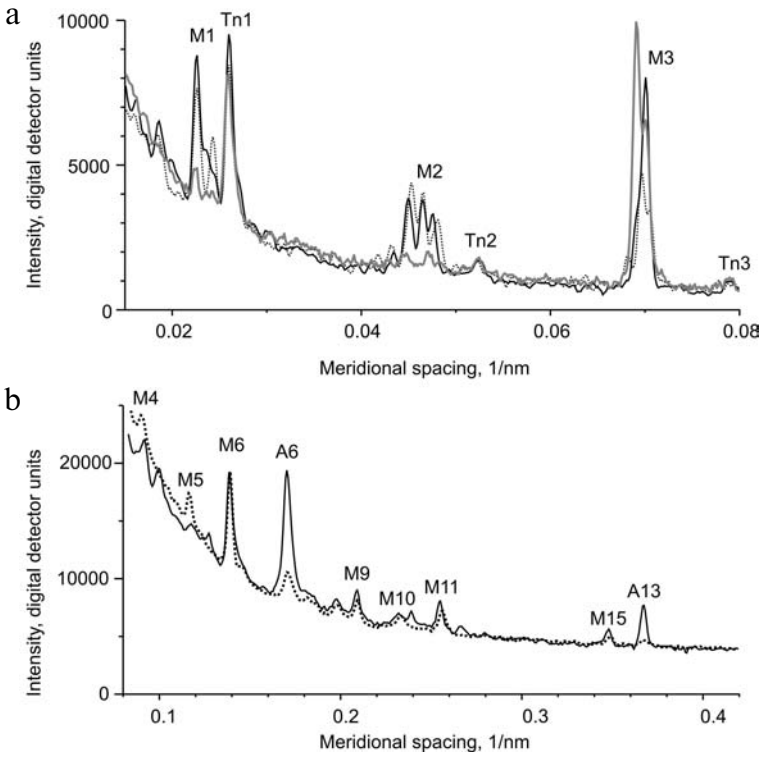

Fig. 12. Distribution of meridional diffraction intensity on rabbit muscle in different states. Intensity distribution along the meridian on X-ray diffraction patterns of thin bundles of rabbit muscle in relaxed state (dotted line), in rigor at low tension (black), and during isometric contraction at ~30°C (gray line). Data were collected at beamline ID02 of ESRF, camera length 10 m (a) and 2.5 m (b); experimental data are described in our work [101] in more detail. Indexes A, M, and Tn correspond to actin, myosin, and troponin reflections.

9). The brightest myosin reflection M3 corresponds to axial periodicity of the myosin head crowns on the thick filament backbone. If myosin filaments were an ideal three-strand helix in which each crown of myosin heads is turned relative to the previous one by 40° and is shifted along the axis by fixed distance ~14.3 nm, the observed meridional reflections would have indexes divisible by 3: M3, M6, M9, etc. [82]. Indeed, there are also different meridional reflections M1, M2, M4, M5, etc., called forbidden because they are caused by the deviations of thick filament from ideal three-strand helix. Forbidden reflections are very well seen on the diffraction pattern of relaxed muscle; they are less bright in rigor and extremely weak in isometric contraction (Fig. 10).

Deviations from three-strand symmetry were ascribed to the effect of protein C on the thick filament structures [104, 105]. The protein C or MyBP-C is the myosin-binding protein present in the form of 7-9 rings on the backbone of thick filament in the zone of overlapping with actin in the case of sarcomere physiological length with period very close to or coinciding with that of M1 [82]. Recent experiments on heart muscle of mice with knockout of MyBP-C-encoding gene have shown that only reflections multiple of M3 are characteristic of such thick filaments, whereas forbidden reflections disappear, i.e. the structure approaches regular three-strand helix [33].

The thick filament axial period estimated from the position of the brightest reflection M3 is 14.34 nm in resting frog muscle, 14.42 nm in rigor [106], and 14.56 nm during isometric contraction [107]. Similar up to 1.5% changes in positions upon activation were registered for M6 and myosin reflections of higher orders [97, 98, 107-109]. Such structural changes are evidently caused not by extension of myosin filaments in response to the external force, but rather by rearrangement of the thick filament backbone upon activation. The nature of this phenomenon is still unknown. The dependence of changes in the myosin reflection positions on the sarcomere length is rather complicated. When relaxed muscle was extended to the sarcomere lengths at which thick and thin filaments almost do not overlap, coordinates of high order myosin reflections (M6, M9, and M15) increased by 0.4-0.8% [98]. At these sarcomere lengths, electric stimulation also did not cause changes in the reflection positions, although at the sarcomere lengths when overlapping is half-maximal, an increase in the reflection positions by ~1% was observed [98]. When muscle or single fibers contracting at full filament overlap were allowed to shorten in response to a low load, spacing of M3 (and M6) partially returned to their values in relaxed muscle (to 14.4-14.45 nm for M3 [109, 110]).

It is believed that in a contractile muscle only myosin heads, both actin-bound and unbound, contribute to the M3 intensity, I_{M3} [48]. The linear decrease in I_{M3} with reduction in the overlap zone upon fiber extension to long sarcomere length has shown that attached heads made the main contribution to this reflection [111]. Many authors believe that M6 and higher order myosin reflections originate from the thick filament backbone structures, different from myosin heads, and therefore changes in the reflection positions can be used for determination of the thick filament compliance [48, 112-114]. Others believe that all myosin reflections include a significant contribution from the heads [115, 116]. The increase in M6 intensity by 60% after step-wise shortening and 25% decrease after step-wise extension [113, 117], or during shortening at maximal velocity [110] show that both heads and the thick filament backbone contribute to M6 intensity, and therefore nothing should be ignored in interpreting the results of measurements of the reflection positions and intensity.

There have been attempts to estimate the thick filament elastic extensibility by imposing on the contractile muscle or to single muscle fibers step-wise length changes whose time (~0.1 msec) is significantly shorter than the characteristic time of the head detachment-reattachment and even than the force-generating step of the myosin cross-bridge. At the end of step-wise fiber shortening, S_{M3} in a single intact frog fiber declined by $0.14\%/T_0$ ([3], here and below S_X means periodicity in physical space, which corresponds to the observed meridional coordinate of reflection X in inverse space). At the end of the phase of rapid partial tension recovery (or phase 2 according to [44]) the S_{M3} decrease was even more pronounced – $0.34\%/T_0$ [3]. For single fiber of *m. tibialis anterior* of the frog *Rana temporaria* at 4°C T_0 is 280-290 kPa. Similar changes by $0.33\text{-}0.36\%/T_0$ were found for S_{M3} in later phases of responses to shortening and in experiments on whole frog muscle [113].

The value of thick filament compliance of $0.26\%/T_0$ was obtained by measuring M6 position in experiments with rapid load changes [112, 113]. It should be noted that changes in positions of myosin meridional reflections can be caused by two factors: (a) changes in the ~14.5 nm axial period of myosin head crowns along the thick filament backbone and (b) length changes of actin filaments to which myosin heads are attached, which contribute to the corresponding reflection intensity. Interpretation of these changes may be even more complicated if myosin heads undergo conformational changes during step-wise change of fiber length and/or load. The estimations of the compliance by M6 and high order reflection measurements may be more correct, although, as indicated above, the contribution of attached myosin heads to intensities of these reflections cannot be excluded.

In the case of isometric tetanus development in intact fiber [109, 110] or in whole frog muscle [48, 118], at the beginning I_{M3} decreases and then increases again. These changes in I_{M3} are accompanied by increase in its radial width (Fig. 13). It was supposed that the increase in the reflection width is caused by higher lateral disordering

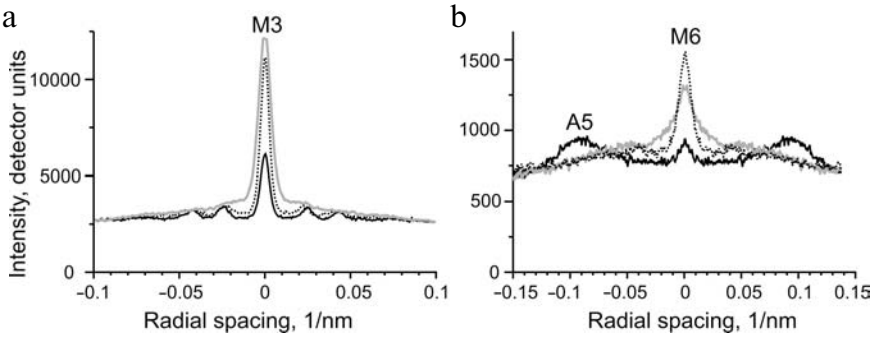

Fig. 13. Radial distribution of reflection M3 (a) and M6 (b) intensity profiles. Data were obtained on a single fiber from rabbit *m. psoas* in relaxed state (dotted line), in rigor (black line), and during isometric contraction at 5°C (gray line). a) I_{M3} distribution in one half of the X-ray diffraction pattern; b) M6 distributions averaged over four quadrants. In relaxed state and in rigor "crystal" reflections corresponding to radial position of equatorial reflections 1,0 and 1,1 are also seen on the profile of layer line M3. The same data as for Fig. 12b. Off-meridional peaks on the layer line M6 in rigor are due to partial contribution to integral profile of layer line A5, whose position is very close to but does not coincide with the axial position of M6.

of thick filaments [118]. In relaxed frog muscle the width of M3 corresponds to the lateral size of coherently diffracting structure about 400 nm, which approximately corresponds to the myofibril radius [106]. Upon contraction the M3 width almost doubles because active forces cause disordering of thick filaments inside myofibril, i.e. they decrease the size of the coherently diffracting region ([118], Fig. 13a).

To correct the observed integral intensity for the effect of disorder, it was proposed to multiply the observed I_{M3} by the reflection radial width measured as radius in reciprocal space at which M3 intensity reaches half of its maximal value [118]. After such correction I_{M3} of contracting muscle significantly increases [110, 118]. Axial disorder of myosin filaments corresponds to disorder of the second kind, so that the filament axial ordering effect on the meridional reflection intensity can be expressed quantitatively.

For example, increase in temperature of intact contracting frog fiber from 2 to 17°C results in only 11% increase of observed I_{M3}. After correction for the width change this value increases to 30%, i.e. it becomes close to the relative increment of developed tension [119]. Similar values for the temperature-dependent increase in I_{M3} were obtained in contracting skinned frog fibers in which the actin–myosin lattice was stabilized by partial cross-linking by ethyldimethyl carbodiimide (EDC) [120]. More pronounced 60% increment in I_{M3} was obtained in experiments with temperature jump from 5 to 30°C on rabbit muscle fibers [78]. The temperature dependence of tension developed by the fiber is steeper for rabbit (warm-blooded) muscle than for frog (cold-blooded) muscle. At the same time, the portion of actin-bound myosin heads estimated by measurement of instant stiffness is independent of the animal muscle temperature in both cases [121, 122]. To generalize this, one can say that the increase in M3 intensity correlates with enhancement of mean force developed by a cross-bridge.

The width of meridional reflections in rigor strongly depends on the procedure used to achieve this condition. If one manages to escape development of high tensions and resulting axial disordering of filaments, M3 profiles in rigor may have the same width as in relaxed muscle and reflections formed by planes (1,0) and (1,1) are also expressed on this profile (Fig. 13a).

Changes in M3 intensity in contracting muscle in response to external mechanical effects are interpreted as a result of a tilt of the whole myosin head around the binding site on actin [48, 49] or only of the S1 light chain domain relative to the catalytic domain of the head [3, 123, 124]. Such interpretation is correct only if head detachment and attachment are slower than changes in M3. Otherwise, the change of the number of attached heads and/or dispersion of their distribution will result in significant changes in I_{M3} [125]. So, the following factors influence intensity of M3 and, probably, of different myosin reflections: the number of actin-bound myosin heads, their shape, the standard deviation from the 14.5 nm axial period, and axial disordering of adjacent myosin filaments.

An interesting effect of meridional reflection splitting to two and more peaks was noted already in early experiments on whole frog muscle using laboratory X-ray sources [106]. It was soon supposed that such splitting of meridional reflections could be due to interference of X-rays scattered by the two symmetrical halves of the sarcomere [126, 127]. Later Malinchik and Lednev obtained X-ray diffraction patterns of resting frog muscle at high spatial resolution and proposed a thick filament model that reproduced the main features of X-ray diffraction pattern including interference splitting of myosin meridional reflexes [128-130]. Bordas et al. [108] considered this effect in experiments on whole muscle with a syn-

chrotron radiation source. They supposed that, as became clear later by mistake, that this reflection was caused by two sets of myosin heads with close but different periodicity.

Layer Lines

Myosin layer lines. Myosin layer lines are parallel to the equator at distances multiple to the myosin helix main period 14.3 nm^{-1}. In frog muscle at rest the intensity of all myosin layer lines is very high [106]. In this state heads of myosin molecules are packed close to the thick filament backbone [106, 130, 131]. In muscle of warm-blooded animals intensities of myosin layer lines at low temperature (about 5°C) are significantly lower due to disorder of myosin heads, but they increase to levels characteristic of cold-blooded animals as temperature increases to 20°C and higher [89, 132-134]. Such transition from disorder to order upon increase in temperature is associated with ATP hydrolysis [89, 134] or more exactly, with transition of myosin heads, with bound ATP or ADP and P_i, from "open" to "closed" state [135]. It appeared that the head in the "closed" state is localized mainly on the thick filament backbone, and there it contacts the paired head of the same molecule, forming an ordered structure [136], whereas heads in the open state leave the thick filament backbone and are disordered. Temperature increase or the use of ATP analogs shift the equilibrium between the two states [135, 137]. Treatment of a fiber with N-ethylmaleimide, fixing S1 in the open state, results in decrease in intensities of myosin layer lines [138]. In rigor off-meridional intensities of myosin meridional reflections are lower than in relaxed muscle, although some of them, including M2, M3, and M6, remain appreciable (Fig. 12) [106, 108].

In the course of isometric contraction, intensities of forbidden myosin meridional reflections M1, M2 and extra-meridional myosin layer lines strongly decrease compared to relaxed state (Fig. 12) [108, 118]. In isometric tetanus of frog muscle at low temperature, the M1 off-meridional intensity is about 15% of its value in the relaxed state [108]. Even lower relative I_{M1} values were found upon isometric contraction of single intact frog fibers [109]. If a contracting muscle is allowed to shorten under low load, then I_{M1} is approximately three times higher than in isometric contraction, although it is only about half of its value in the relaxed state [99]. Since the fraction of bound myosin heads falls during rapid shortening of contracting muscle [139, 140], these data show that the off-meridional part of M1 and possibly the off-meridional parts of different myosin layer lines in contracting muscle mainly result from X-ray diffraction on detached myosin heads.

On the other hand, there are data indicative of a significant contribution to myosin layer lines of weakly bound myosin heads containing in their active center either ATP [141] or ADP·P_i [142]. To estimate the contribution of weakly bound and detached heads to the intensity of different X-ray reflections, skinned muscle fibers were placed under conditions that change the fractions of strongly and weakly bound, or bound and detached heads, and changes in X-ray diffraction patterns were recorded [141, 142].

Actin layer lines. Actin layer lines correspond to helix with period ~1/36 nm^{-1} (Fig. 9). The simplest model describes the main actin reflections: meridional reflection at $(2.73\ nm)^{-1}$, bright layer lines with axial position $\sim(5.9\ nm)^{-1}$ and $\sim(5.1\ nm)^{-1}$ that remain bright even in the relaxed state of the muscle, and of the first layer line at $(\sim 36\ nm)^{-1}$, it is the integral model 13/6. This model is approximate because actin filament is very motile and in reality it is neither integral helix nor even truly periodical structure [143]. This is confirmed by experimental observations showing that the width of the actin layer lines is much higher than that of myosin layer lines (Fig. 10). For different states of thin filaments or oriented F-actin gels, different integer but more complex models are used such as 67/31, 132/61, or 69/32 [144]. In this section we shall hold on the simplest nomenclature in which A1 corresponds to the first actin layer line at $\sim(36\ nm)^{-1}$ while A6 and A7 correspond to layer lines with axial positions $\sim(5.9\ nm)^{-1}$ and $\sim(5.1\ nm)^{-1}$, respectively.

It is known that F-actin structure strongly depends on many factors. Changes in intensities of A1, A2, and A6 actin layer lines [53, 145] as well as of their positions indicative of changes in axial pitch and angle between adjacent actin monomers in the helix [98, 99] were registered immediately after beginning of intact muscle electric stimulation, i.e. under conditions when myosin heads still have no time to bind actin, as well as in the case of maximally rapid muscle shortening causing disconnection of most heads from actin. Strong binding of myosin heads to actin also extends and twists the actin helix even in the absence of external extending force [101].

On X-ray patterns of relaxed muscle actin layer lines, with the exception of A6 and A7, are weak. This is because myosin heads are near thick filaments and do not contribute to effective electron density of thin filaments.

All actin layer lines become very bright in rigor because in this state all myosin heads strongly and stereospecifically bind actin, thus making contrast in the actin helix (Fig. 10) [106]. Rigor values of layer line intensities are often used to scale intensities in different physiological or biochemical states. Even higher intensity of actin layer lines can be obtained after addition of isolated myosin heads to solution bathing skinned fibers. To do this, fibers are extended to sarcomere length of 3-4 μm and incubated in solution containing S1 [146, 147].

Whereas S1 without nucleotide or S1·ADP complex strongly bind actin, S1 complex with ATP or ADP and P_i exhibit weaker affinity to actin [38]. The state of weak binding of S1 to actin is still poorly studied. It was shown that upon lowering ionic strength of the relaxing solution

surrounding skinned fibers treated with N-phenylmaleimide, the intensity of the first layer line I_{A1} decreases [141]. Such treatment stops ATP hydrolysis and leaves myosin heads in conditions when only weak binding to actin is possible. Besides, it is known that low ionic strength stimulates weak binding of myosin heads to actin [148]. In this case no changes in I_{A6} were found, which suggests that the weak binding is not stereospecific [141, 149, 150]. Such attachment is possible within a broad range of axial and azimuthal angles between actin monomer and myosin head. Since weak binding is sensitive to ionic strength [148], its nature is, most likely, electrostatic.

In early synchrotron experiments with mainly one-dimensional detectors, no noticeable changes in I_{A1} were found upon development of contraction [48]. The model for explanation of this effect was based on the supposition that during contraction a significant fraction of myosin heads are weakly bound to actin [151]. When two-dimensional detectors became available, it became possible to register I_{A1} increase during isometric contraction compared to that at rest [152]. Due to good X-ray focusing (stations 2.1 and 16.1, SRS, Great Britain) and use of a long chamber, X-ray patterns with good spatial resolution were obtained. It became possible to distinguish reliably close peaks M1 and A1 of the first axial layer line in contractile muscle and to measure their intensity in different states [108].

In a frog muscle contracting at low temperature, I_{A1} is 10-15% of its level in rigor [120]. As the temperature of contracting muscle increased, I_{A1} increased approximately in proportion with increase of tension, although the number of actin-bound myosin heads remained unchanged judging by measurements of dynamic stiffness of fibers and intensity of equatorial reflection 1,1 [120-122]. In the course of isometric contraction at high temperature, I_{A1} in frog muscle was about one third of its level in rigor [120]. In the case of shortening under low load, i.e. at the velocity close to maximal, I_{A1} approximately halved [99] in parallel with decrease in number of actin-bound myosin heads [153]. Other actin layer lines A2, A4, and A5 are also seen on X-ray pattern, although their intensities are much lower than in rigor [108].

Actin–myosin layer lines. There are two rather bright layer lines on X-ray diffraction pattern of muscle in the rigor state. The periods of these lines ~23-24 and ~10.2-10.4 nm coincide neither with myosin nor with actin based periodicities [106]. These layer lines were not found on X-ray pattern of relaxed muscle, but emerged upon contraction when muscle develops force [108] (Fig. 10). Yagi explained the presence of these layer lines by modulation of function of myosin head binding to actin filaments with thick filament period 14.5 nm and suggested theoretical explanation of this event [154]. The modulation results in appearance of layer lines at $1/14.5 - 1/36 = \sim 1/24$ nm^{-1} for the layer line designated as AM_{-1} and $1/14.5 + 1/36 = \sim 1/10.4$ nm^{-1} for AM_{+1}, where 36 nm is the conventional period of the actin filament. Neither detached heads nor thin filaments contribute to these layer lines. Exact solution of the problem concerning diffraction on partially filled integral rational helix is given in [155].

MODELS OF X-RAY DIFFRACTION ON MUSCLE

Interpretation of muscle X-ray diffraction patterns is impossible without mathematical models. First data on helical structure of thick and thin filaments were obtained from X-ray diffraction patterns using the known solution of the problem concerning diffraction on helix, which was used for solving DNA structure [156].

Modeling of Equatorial Reflections

The brightest equatorial reflections are caused by diffraction on the planes (1,0) and (1,1) (Fig. 9). Changes in intensities of these reflections were associated with change of the fraction of actin-bound myosin heads without carrying out digital analysis [83, 157]. If myosin heads are laid near the thick filament backbone, then scattering mass is concentrated in planes (1,0) passing only through thick filaments, while in planes (1,1), passing through thin and thick filaments in proportion 2 : 1, contribution of the head mass is significantly lower; therefore, $I_{1,0} > I_{1,1}$. This situation is observed in relaxed muscle. In contrast, if all heads of myosin molecules are attached to thin actin filaments, then $I_{1,1}$ increases and $I_{1,0}$ decreases. This situation is observed in rigor. In contracting muscle only a fraction of myosin heads are actin-bound and develop active force, and due to this the $I_{1,1}/I_{1,0}$ ratio is intermediate between the considered extreme cases.

Actin filaments are kept in points of the hexagonal lattice only due to interaction with the closest thick filaments. In relaxed muscle myosin heads do not bind actin but just push them from three sides, in active state and in rigor heads bind actin and therefore they better control the order of the actin lattice [92]. Thus, in the overlap zone disorder in thin filaments is of the first kind, which suggests random deviations from ideal positions within the lattice. For this type of disorder, equatorial intensity will be multiplied by thermal factor $T_R = \exp(-4\pi^2\Delta_{AR}{}^2R^2)$, where Δ_{AR} and R are the root-mean-square actin filament deviation from the ideal position (Fig. 14) and the radial coordinate in reciprocal space, respectively [158]. In this case intensity distribution within a reflection is independent of Δ_{AR}, and the whole reflection intensity is multiplied by T_R. Model calculations have shown that it is possible to reproduce quantitatively the $I_{1,1}/I_{1,0}$ ratio if we assume significant disorder of the thin filament (Δ_{AR} up to 3 nm), especially for cold-blooded animals frog or fish, in which

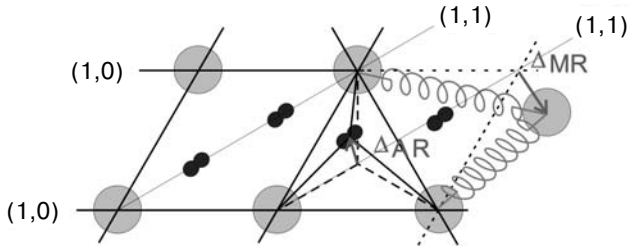

Fig. 14. Distortions in the actin–myosin lattice regularity.

$I_{1,1}$ is especially low (Fig. 11). This conclusion agrees well with electron microphotographs of thin slices of relaxed rabbit fibers at high temperature, on which significant uncorrelated disorder of thin filaments is seen [91] and the $I_{1,1}/I_{1,0}$ ratio is almost the same as in frog muscle.

Thick filaments are kept in the lattice points by M line proteins and possibly by different sarcomere proteins that prevent their shift in axial and radial directions. This structure may exhibit the second kind disorder characterized by the absence of long range order, and the distance to the closest neighbor obeys some fixed distribution with a certain root-mean-square deviation from the mean value. Such disorder is characterized by reflection widening with increase in reflection index [158]. In fact, on the muscle X-ray pattern reflection 1,1 is somewhat wider than 1,0, while the higher order reflections are even wider (Fig. 11). These data confirm the observation that both the first and second kinds of disorders are present in the actin–myosin lattice; it is very difficult to determine parameters of these disorders on the basis of experimental data. There have been several attempts to restore projection of electron density to the equatorial plane using Fourier synthesis (for example, [88, 159, 160]), but it appeared that the result of modeling strongly depends on poorly determined parameters such as phases of equatorial reflections. Thus, the use of equatorial reflections for quantitation of actin–myosin interaction was not very successful.

Modeling the Diffraction Diagram of Relaxed Muscle

The first spatial muscle model, considering all then known data on the thick filament geometry, was proposed by Malinchik and Lednev for interpretation of an X-ray diffraction pattern of relaxed muscle [129, 130]. They parameterized deviations of myosin head positions on the thick filament backbone caused by MyBP-C from the ideal ones, corresponding to the helix axial period, and optimized the choice of parameters by comparing results of calculations on model with the experimental profile of meridional intensity. This allowed them to explain the appearance of forbidden meridional reflections on the X-ray pattern of relaxed skeletal muscle. Moreover, they proposed the thick filament model using the myosin head approximations by a series of adjacent spheres. Disordering the myosin filament packing to hexagonal cells was described as the second kind disorder. This model was used to calculate intensities of myosin layer lines and compare them with experimental ones. This comparison made possible approximate estimation of myosin head distribution near the thick filament backbone.

A set of works by J. Squire (see for example [160-162]) deal with detailed modeling of X-ray patterns of relaxed muscle. To reconstruct myosin heads on the thick filament backbone in the relaxed state, they used X-ray patterns of the flounder fin muscle because in it, like in many different fish muscles, hexagonal package of thick and thin filaments is described by a simple elementary cell, which means that its structure is closer to crystalline. The concept was used to interpret X-ray patterns of the muscle in different states and design a movie reproducing motility of myosin heads in active muscle and their positions at rest and in rigor. The state of relaxed muscle became the zero frame. Using data on the myosin lattice disposition in a sarcomere, constantly improving data of electron microscopy followed by data of protein crystallography on the myosin head structure, they designed different structural models of the A zone in relaxed muscle, using a substantial set of parameters that assigned position of myosin heads in space, and compared the results with data of X-ray diffraction [131, 161, 162]. The last of published models contains 24 independent parameters, and the best set provides for squared R factor of 1.19% for 56 reflections [162].

The research group of Leepo Yu at the US National Institute of Health continued in parallel works on modeling diffraction of resting muscle. A former PhD student of V. V. Lednev, S. B. Malinchik, worked for several years in this group. On the basis of current concepts of the myosin head structure, they modeled the thick filament structure taking into account thermal disorder of the first kind of myosin heads. They compared modeling results with experimental data and showed that with increase of the resting muscle temperature, myosin heads are arranged at the thick filament backbone and contrast the myosin helix [133]. The same approach was used in following works of this group for investigation of myosin head positions in resting muscle in different states [142, 150, 163].

Modeling X-Ray Patterns of Active Contraction and Rigor States

Transition from “frame zero” to modeling the states in which myosin heads are bound to actin, namely, states of active contraction and rigor, is more complicated, first due to necessity to consider complete three-dimensional

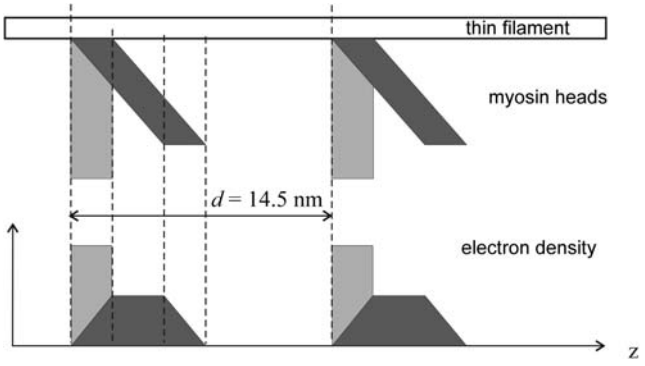

Fig. 15. A simple model of the myosin head working stroke, which explains changes in M3 X-ray reflection in response to the stepwise shortening of the fiber. Above are cross bridges approximated by rectangles, below is a projection of the head electron density onto the fiber axis (according to [49]).

actin–myosin lattice, and second, due to the presence of unknown characteristics of myosin head arrangements on the thin filament. Therefore, to simplify the modeling, either features of distribution of bound myosin heads on actin or the shape of attached heads were usually ignored.

In the first type of models only one efficient myosin head is considered assuming that its electron density is the mean density of all cross bridges and that in the overlap zone of thick and thin filaments myosin heads are bound to actin with the same period equal to the period of the M3 reflection. This model was used for description of changes of meridional reflections M3, M6, and higher orders. The first such model (Fig. 15) gave only a qualitative description of the experimental data [49].

When the atomic structure of S1 and models of actin-myosin binding became available, quantitative calculations of changes in meridional reflection intensities became possible [2]. Changes in the myosin head configurations were calculated using the known crystallographic atomic model of the actin–myosin complex ([164], protein structure database ID PDB 2mys). Conformational changes in myosin head corresponding to the "lever arm tilt" (Figs. 5 and 16) were modeled by the light chain domain (LCD) tilt around the converter in the plane passing through the actin axis and the straight line passing through amino acid residues Cys707 (the hinge between catalytic domain and "lever arm") and Lys843 (point of joint between myosin subfragments S1 and S2). The neck rotation center coincided with coordinates of the C_α atom of amino acid residue Cys707 [60, 62]. The catalytic domain of attached heads was considered as rigid body upon the tilt of the lever arm. Elastic bending of the neck of S1 caused by external forces was calculated using formulas of elastic beam bending [2].

The catalytic domain (amino acid residues 1-770) of bound myosin head remained unchanged, while the neck bent like a beam with uniform bending rigidity, restrained in a point, corresponding to amino acid residue Gly770, controlled by the moment of external force applied to the distal beam end or to amino acid residue Trp829. The beam axis coincided with the straight line passing through Gly770 and Trp829. It was assumed in calculations that each sphere displacement is perpendicular to the beam axis and lies in the plane passing through the beam axis and vector of applied force. The displacement value was calculated using the formula $d_{829}(3L - x)x^2/2L^3$ [165], where $L = 8.47$ nm is the length of the stretch [Gly770-Trp829] or the beam length, x is the distance from Gly770 to the sphere projection to the beam axis, and d_{829} is the displacement of Trp829. We used this model in calculations of I_{M3} intensity changes upon sinusoidal changes in the fiber length in active contraction and in rigor [2].

We recently proposed a structure–kinetic model of the cross bridge work (Fig. 17) [78]. It is based on the following experimental results: the I_{A1} and tension increase in response to temperature jump occur simultaneously [77, 78]; the fiber stiffness in active contraction is temperature independent [121, 122], and no changes in the intensity of reflection 1,1 after temperature jump are observed [77], which suggests that the tension increase with temperature occurs with a constant number of myosin bridges attached to thin filaments. We believe that the rise in intensity of actin layer lines after temperature jump is caused by change in configuration of cross bridge interactions with actin, namely, by their transition from non-stereospecific attachment to stereospecific binding.

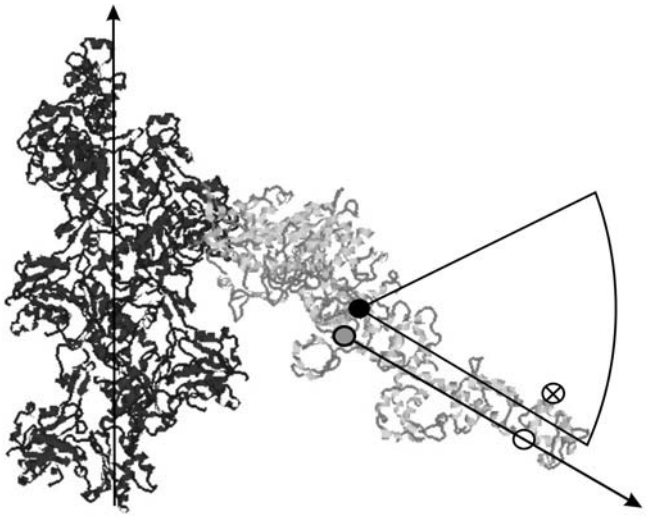

Fig. 16. Model of myosin head strong binding to actin (according to [56]; actin – 1atn.pdb, S1 – 2mys.pdb). Five actin monomers are shown in black on the left, the thin filament axis is shown, the arrow points to the direction towards the M line. Amino acid residues important for modeling of the changes in the head shape are shown by circles: Cys707 is black, Gly770 – gray, Trp829 – open circle, Lys843 – crossed circle. Axis x coincides with the "lever" axis [Gly770, Trp829] (see text).

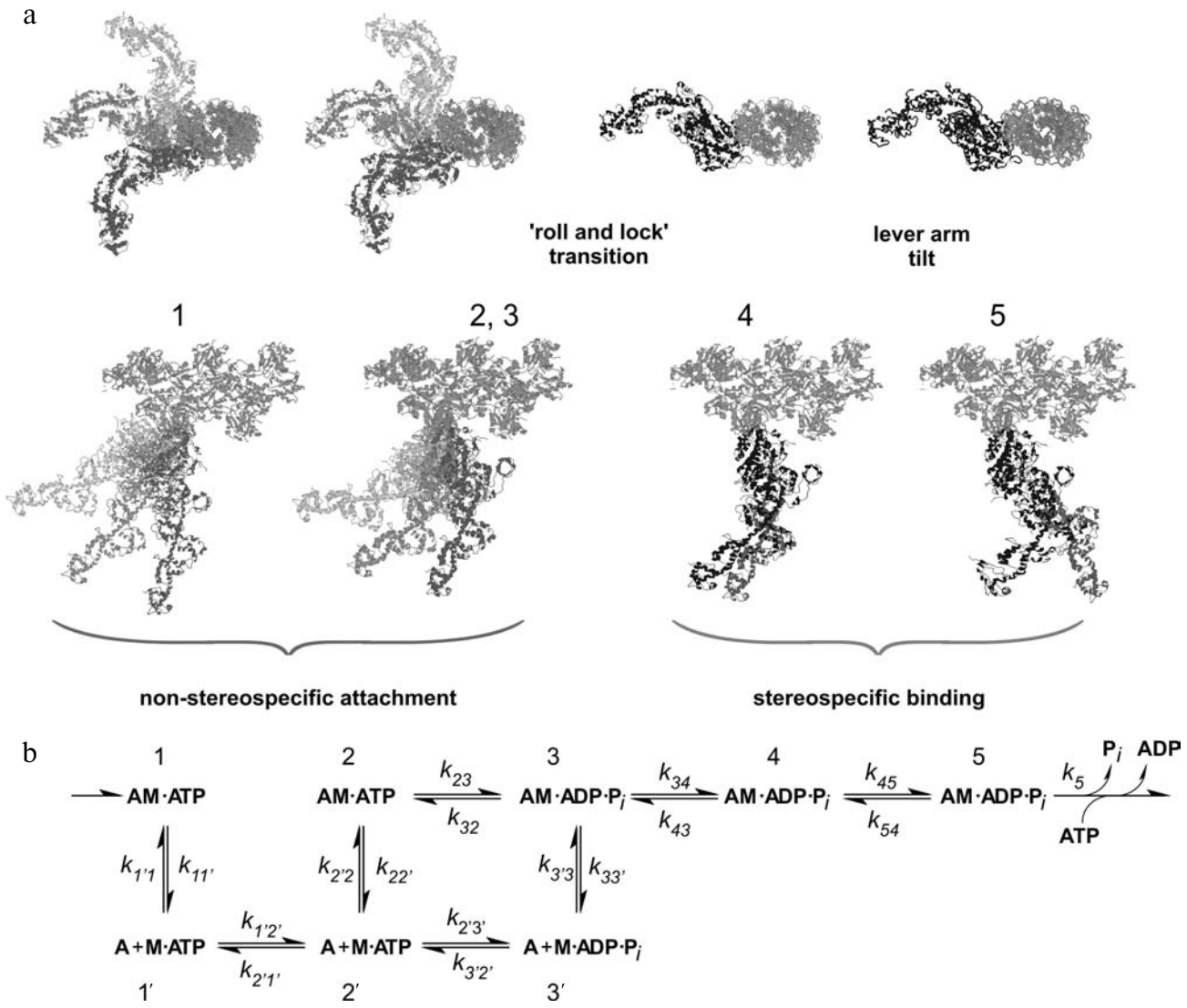

Fig. 17. Structural and kinetic schemes of the mechanism of force generation by myosin molecule heads [78]. a) Different states (1-5) of myosin head (shown in gray and black) bound to actin filament (dark gray) are shown in two projections: in the upper row the actin filament axis is perpendicular, in the lower row it is parallel to the figure plane. In the lower row the sarcomere Z-line is on the right. b) Kinetic scheme of the cross-bridge biochemical cycle used in the model. Pre- and post-hydrolysis states 2 and 3 are structurally identical but biochemically different. In states 1, 2, and 3 heads are rigid in axial direction but they are able to bind actin at different angles in axial and azimuthal directions. The full range of azimuthal and axial angles is ±60° and ±30°, respectively; the figure shows central and extreme positions of the heads. Distribution along azimuthal and axial angles is random and uniform in the whole physical sector. Force or displacement is created both by the "roll and lock" transition (step 3→4) with average axial rotation of subfragment 1 as a solid body by 26° and upon the lever arm tilt (step 4→5) with mean axial rotation by 50° relative to the motor domain. Unstrained shapes of heads in force-generating states 4 and 5 are shown in gray (right position in the pair, the lower row on (a)); strained forms are shown in black (left position). A and M on the kinetic scheme (b) designate actin and myosin subfragment 1, respectively. Heads may reversibly detach from states 1, 2, and 3 to states 1′, 2′, and 3′, respectively.

Synchronous increase in tension and actin helix contrasting by myosin heads shows that stereospecific head "locking" on actin is a necessary phase of cross bridge force generation. The decrease in $I_{1,0}$ with relative stability of $I_{1,1}$ also favors non-stereospecifically attached head transition to stereospecifically bound state, because when the catalytic domain of non-stereospecifically attached head incorporates into actin helix, the tail domain of myosin head departs from the thick filament backbone, thus lowering $I_{1,0}$, although the total mass associated with the thin filament and thus $I_{1,1}$ does not change [120].

The model suggests that before ATP hydrolyzes, the myosin head is able to bind actin only in non-stereospecific manner, i.e. under different axial and azimuthal angles, and its strong binding to actin is possible only after ATP cleavage to ADP and phosphate. In the first three biochemically different states myosin head non-stereospecifically binds actin and does not develop force. After

hydrolysis the head quickly and reversibly "locks" into the stereospecifically bound state and only after that the lever tilts. Both locking and lever arm tilts are force-generating transitions. This model based on the current biochemical concepts of kinetics of ATP hydrolysis by myosin quantitatively explains our experimental data, namely, changes in intensities of X-ray reflection M3 and the first actin layer line A1 in response to temperature jump [78] and includes the lever arm model used by many authors for explanation of changes in M3 intensities in experiments with changes in lengths of actively contracting fibers.

Tomography of electron-microscopic slices of isometrically contracting insect flight muscle, which were obtained by rapid freezing [166, 167], have shown significant differences in motor domain configuration compared to reconstructions of rigor acto-S1 complex. These tomographies show both myosin heads with motor domains bound to actin in approximately the same manner as in rigor complex *in vitro* and their "neck" domains tilted by different angles, as well as heads with catalytic domains bound to actin under different axial and azimuthal angles. These data agree well with our model and additionally show that the mechanism of force development by the actin–myosin motor is more complex than simply a tilt of a long "neck".

Instead of complex and difficult problem of sorting out numerous configurations of attached myosin head, it is possible to set the function of head arrangement on the thin filament and, possibly, their orientation in space using direct modeling of the layer line intensities and known data on the structure of actin–myosin lattice. The first work of this kind was interpreting the X-ray diffraction patterns of insect flight muscle in rigor [168]. The authors considered a single unit cell of actin–myosin lattice on the basis of features of the diffraction pattern, selected a group of spatial symmetry, and checked different assumptions concerning the shape and configuration of attached heads and functions of their arrangement on actin according to preliminary data of electron microscopy. Satisfactory agreement between calculated and experimental data was obtained, which indicated that the cross bridge in rigor is inclined under the angle of approximately 45° to the actin axis, heads interact with about one third of actin monomers, and the most important is that authors of this work proposed for the first time a method for interpretation of the whole two-dimensional X-ray diffraction pattern of the actin–myosin lattice rather than analysis of individual reflections.

Several models were proposed for arrangement of myosin heads in a single unit cell without accounting for their shape [169]. It was shown that myosin heads should bind actin with periodicity of its helix to provide for the presence in X-ray diffraction pattern of the family of bright actin layer lines characteristic of rigor state. If myosin heads are allowed to bind actin monomer closest by the axial coordinate, assuming large azimuthal angles of head tilt, then for such arrangement myosin layer lines will be bright on the X-ray diffraction pattern, i.e. a rule of actin monomer selection may take place upon weak binding.

Models of this kind can be improved using available atomic structures of actin monomer, myosin head, as well as models of strong actin–myosin binding [164, 170] to design direct models of actin–myosin lattice in rigor and active contraction states. The main difficulty in modeling the three-dimensional actin–myosin lattice in the overlap zone of thick and thin filament is that it is necessary to find for each of hundreds of myosin heads, projecting from one of six myosin filaments in an unit cell, that one of hundreds of actin monomers, localized on one of six actin filaments, to which it binds during active contraction or in rigor state. One of approaches to solution of this problem is the use of the "principle of minimum of elastic energy" according to which myosin head binds the actin monomer on one adjacent thin filament for which energy of the myosin head strain needed for such binding, is minimal [171]. From application of this principle, the disposition of myosin heads on the actin filament is defined by just two parameters: the ratio of longitudinal and transverse stiffness of the actin–myosin complex and the fraction of myosin heads bound to actin in this state. Calculations of complete two-dimensional X-ray diffraction pattern, carried out using this model, agreed with the experimental data [125, 171]. This model also revealed on experimental X-ray diffraction pattern the X-ray reflections whose change in intensity allows determination of some characteristics of actin–myosin interaction in muscle: the number of myosin heads stereospecifically bound to actin, their conformation ("lever arm" tilt), axial displacement of center of mass of heads, etc.

Owing to achievements of X-ray crystallography during the past two decades, it has become possible to clarify important details of atomic structure of the main elements of the actin–myosin motor in muscle such as monomeric and fibrillar actin and myosin head in different structural and biochemical states. Data on the structure of the actin–myosin complex obtained using modern electron microscopy exhibit lower resolution and make it possible to characterize only a single stage of myosin interaction with actin and ATP, a stable complex formed after release of the ATP hydrolysis products from the active center of the head. Data on the character of structural rearrangement of actin–myosin complex, which underlie muscle contraction, are still fragmentary and incomplete. One of traditional methods of ultrastructural investigation of striated muscle is low-angle X-ray diffraction. Owing to development of third generation synchrotron radiation sources and rapid detectors, this method is useful because it makes it possible to obtain structural information on motility of myosin heads in contractile muscle with temporal resolution up to 20 μsec and spatial resolution of some diffraction reflections up to 0.2 nm.

Although X-ray diffraction experiments serve as a rich source of information, analysis of their data in terms of molecular movements requires development of mathematical models and their parametric analysis. One may hope that these data together with new results obtained by methods of modern biochemistry combined with point mutations in the main contractile proteins will help in restoration of the pattern of biochemical and structural changes forming the basis of mechanochemical energy transformation by the actin–myosin motor.

This work was supported by the Russian Foundation for Basic Research (grant 11-04-00908-a).

REFERENCES

1. Huxley, H. (1951) *Disc. Faraday Soc.*, **11**, 148.
2. Dobbie, I., Linari, M., Piazzesi, G., Reconditi, M., Koubassova, N., Ferenczi, M. A., Lombardi, V., and Irving, M. (1998) *Nature*, **396**, 383-387.
3. Piazzesi, G., Reconditi, M., Linari, M., Lucii, L., Sun, Y. B., Narayanan, T., Boesecke, P., Lombardi, V., and Irving, M. (2002) *Nature*, **415**, 659-662.
4. Kuehne, W. (1859) *Archiv fur Anatomie, Physiologie und Wissenschaftliche Medicin*, 748-835.
5. Schipiloff, C., and Danilewsky, A. (1881) *Vertheilung in Muscelbundel (Hoppe-Seyl. Z.)*, **5**, 349-365.
6. Huxley, A. F. (1980) *Reflections on Muscle. The Sherrington Lectures XIV*, University Press, Liverpool.
7. Engelhardt, W. A., and Lyubimova, M. N. (1939) *Nature*, **144**, 668-669.
8. Engelhardt, W. A., and Lyubimova, M. N. (1939) *Biokhimiya*, **4**, 716-736.
9. Straub, F. (1943) *Actin Studies from the Institute of Medical Chemistry, University of Szeged* (reprinted by S. Karger, Basel-New York), **2**, 3.
10. Szent-Györgyi, A. (1951) *Nature*, **167**, 380-381.
11. Hanson, J., and Huxley, H. E. (1953) *Nature*, **172**, 530-532.
12. Huxley, A. F., and Niedergerke, R. M. (1954) *Nature*, **173**, 971-973.
13. Huxley, H. E., and Hanson, J. (1954) *Nature*, **173**, 973-976.
14. Filatov, V. L., Katrukha, A. G., Bulargina, T. V., and Gusev, N. B. (1999) *Biochemistry (Moscow)*, **64**, 969-985.
15. Gusev, N. B. (2000) *Soros's Edu. J.*, **6**, 24-32.
16. Bailey, K. (1948) *Biochem. J.*, **43**, 271-279.
17. Li, X. E., Holmes, K. C., Lehman, W., Jung, H., and Fischer, S. (2010) *J. Mol. Biol.*, **395**, 327-339.
18. Frye, J., Klenchin, V. A., and Rayment, I. (2010) *Biochemistry*, **49**, 4908-4920.
19. Ebashi, S. (1963) *Nature*, **200**, 1010.
20. Ebashi, S., and Ebashi, F. J. (1964) *Biochemistry*, **55**, 604-613.
21. Ebashi, S., and Kodama, A. (1965) *J. Biochem.*, **58**, 107-108.
22. Huxley, H. (1972) *Cold Spring Harb. Symp. Quant. Biol.*, **37**, 361-376.
23. Haselgrove, J. (1972) *Cold Spring Harb. Symp. Quant. Biol.*, **37**, 341-352.
24. Parry, D. A., and Squire, J. M. J. (1973) *Mol. Biol.*, **75**, 33-55.
25. Ebashi, S., and Kodama, A. J. (1966) *Biochemistry*, **59**, 425-426.
26. Solov'yova, O. E., Katsnelson, L. B., Konovalov, P. V., and Markhasin, V. S. (2006) *Modern Problems in Biomechanics* [in Russian], MGU Publishing House, Moscow, Vol. 11, pp. 131-151.
27. Poglazov, B. F., and Levitskii, D. I. (1982) *Myosin and Biological Motility* [in Russian], Nauka, Moscow.
28. Cope, M., Whisstock, J., Rayment, I., and Kendrick-Jones, J. (1996) *Structure*, **4**, 969-987.
29. Foth, B. J., Goedecke, M. C., and Soldati, D. (2006) *Proc. Natl. Acad. Sci. USA*, **103**, 3681-3686.
30. Margossian, S. S., and Lowey, S. J. (1973) *Mol. Biol.*, **74**, 301-311.
31. Margossian, S. S., and Lowey, S. J. (1973) *Mol. Biol.*, **74**, 313-330.
32. Podlubnaya, Z. A. (1987) in *Structure and Functions of Contractile System Proteins* [in Russian], Leningrad, pp. 32-70.
33. Luther, P. K., Bennett, P. M., Knupp, C., Craig, R., Padron, R., Harris, S. P., Patel, J., and Moss, R. L. (2008) *J. Mol. Biol.*, **384**, 60-72.
34. Huxley, H. E. (1957) *J. Biophys. Biochem. Cytol.*, **3**, 631-648.
35. Huxley, H. E. (1958) *Sci. Am.*, **199**, 67-72.
36. Reedy, M. K., Holmes, K. C., and Tregear, R. T. (1965) *Nature*, **207**, 1276-1280.
37. Huxley, H. E. (1969) *Science*, **164**, 1356-1365.
38. Lymn, R. W., and Taylor, E. W. (1971) *Biochemistry*, **10**, 4617-4624.
39. Bagshaw, C. R., and Trentham, D. R. (1974) *Biochem. J.*, **141**, 331-349.
40. Zoghbi, M. E., Woodhead, J. L., Moss, R. L., and Craig, R. (2008) *Proc. Natl. Acad. Sci. USA*, **105**, 2386-2390.
41. Stewart, M. A., Franks-Skiba, K., Chen, S., and Cooke, R. (2010) *Proc. Natl. Acad. Sci. USA*, **107**, 430-435.
42. Cooke, R. (1986) *CRC Crit. Rev. Biochem.*, **21**, 53-118.
43. Holmes, K. C. (1997) *Curr. Biol.*, **7**, R112-118.
44. Huxley, A. F., and Simmons, R. M. (1971) *Nature*, **233**, 533-538.
45. Rosenbaum, G., Holmes, K. C., and Witz, J. (1971) *Nature*, **230**, 434-437.
46. Huxley, H. E., and Holmes, K. C. (1997) *J. Synchrotron Radiat.*, **4**, 366-379.
47. Huxley, H., Simmons, R., Faruqi, A., Kress, M., Bordas, J., and Koch, M. (1981) *Proc. Natl. Acad. Sci. USA*, **78**, 2297-2301.
48. Huxley, H. E., Simmons, R. M., Faruqi, A. R., Kress, M., Bordas, J., and Koch, M. H. (1983) *J. Mol. Biol.*, **169**, 469-506.
49. Irving, M., Lombardi, V., Piazzesi, G., and Ferenczi, M. A. (1992) *Nature*, **354**, 156-158.
50. Sheetz, M. P., and Spudich, J. A. (1983) *Nature*, **303**, 31-35.
51. Yanagida, T., Nakase, M., Nishiyama, K., and Oosawa, F. (1984) *Nature*, **307**, 58-60.
52. Kron, S. J., and Spudich, J. (1986) *Proc. Natl. Acad. Sci. USA*, **83**, 6272-6276.
53. Kress, M., Huxley, H. E., Faruqi, A. R., and Hendrix, G. J. (1986) *Mol. Biol.*, **188**, 325-342.
54. Kabsch, W., Mannherz, H. G., Suck, D., Pai, E. F., and Holmes, K. C. (1990) *Nature*, **347**, 37-44.
55. Holmes, K. C., Popp, D., Gebhard, W., and Kabsch, W. (1990) *Nature*, **347**, 44-49.
56. Rayment, I., Holden, H. M., Whittaker, M., Yohn, C. B., Lorenz, M., Holmes, K. C., and Milligan, R. A. (1993) *Science*, **261**, 50-58.
57. Oda, T., Iwasa, M., Aihara, T., Maeda, Y., and Narita, A. (2009) *Nature*, **457**, 441-445.

58. Fisher, A. J., Smith, C. A., Thoden, J. B., Smith, R., Sutoh, K., Holden, H. M., and Rayment, I. (1995) *Biochemistry*, **34**, 8960-8972.
59. Smith, C. A., and Rayment, I. (1996) *Biochemistry*, **35**, 5404-5417.
60. Dominguez, R., Freyzon, Y., Trybus, K. M., and Cohen, C. (1998) *Cell*, **94**, 559-571.
61. Houdusse, A., Kalabokis, V. N., Himmel, D., Szent-Györgyi, A. G., and Cohen, C. (1999) *Cell*, **97**, 459-470.
62. Houdusse, A., Szent-Györgyi, A. G., and Cohen, C. (2000) *Proc. Natl. Acad. Sci. USA*, **97**, 11238-11243.
63. Bauer, C. B., Holden, H. M., Thoden, J. B., Smith, R., and Rayment, I. (2000) *J. Biol. Chem.*, **275**, 38494-38499.
64. Coureux, P.-D., Wells, A. L., Menetrey, J., Yengo, C. M., Morris, C. A., Sweeney, H. L., and Houdusse, A. (2003) *Nature*, **425**, 419-423.
65. Sweeney, H. L., and Houdusse, A. (2004) *Philos. Trans. R. Soc. Lond. B.*, **359**, 1829-1841.
66. Sweeney, H. L., and Houdusse, A. (2010) *Cell*, **141**, 573-582.
67. Yang, Y., Gourinath, S., Kovacs, M., Nyitray, L., Reutzel, R., Himmel, D. M., O'Neall-Hennessey, E., Reshetnikova, L., Szent-Györgyi, A. G., Brown, J. H., and Cohen, C. (2007) *Structure*, **15**, 553-564.
68. Manstein, D. J., Ruppel, K. M., and Spudich, J. A. (1989) *Science*, **246**, 656-658.
69. Geeves, M. A., and Holmes, K. C. (2005) *Adv. Protein Chem.*, **71**, 161-193.
70. Uyeda, T. Q., Abramson, P. D., and Spudich, J. A. (1996) *Proc. Natl. Acad. Sci. USA*, **93**, 4459-4464.
71. Reubold, T. F., Eschenburg, S., Becker, A., Kull, F. J., and Manstein, D. J. (2003) *Nat. Struct. Biol.*, **10**, 826-830.
72. Conibear, P. B., Bagshaw, C. R., Fajer, P. G., Kovacs, M., and Malnasi-Csizmadia, A. (2003) *Nat. Struct. Biol.*, **10**, 831-835.
73. Malnasi-Csizmadia, A., Woolley, R. J., and Bagshaw, C. R. (2000) *Biochemistry*, **39**, 16135-16146.
74. Malnasi-Csizmadia, A., Pearson, D. S., Kovacs, M., Woolley, R. J., Geeves, M. A., and Bagshaw, C. R. (2001) *Biochemistry*, **40**, 12727-12737.
75. Bagshaw, K. (1985) *Muscle Contraction* [Russian translation], Mir, Moscow.
76. Huxley, H. E. (1953) *Proc. R. Soc. Lond. B*, **141**, 59-62.
77. Bershitsky, S. Y., Tsaturyan, A. K., Bershitskaya, O. N., Machanov, G. I., Brown, P., Burns, R., and Ferenczi, M. A. (1997) *Nature*, **388**, 186-190.
78. Ferenczi, M. A., Bershitsky, S. Y., Koubassova, N., Siththanandan, V., Helsby, W. I., Panine, P., Roessle, M., Narayanan, T., and Tsaturyan, A. K. (2005) *Structure*, **13**, 131-141.
79. Tsaturyan, A. K., Bershitsky, S. Y., Burns, R., He, Z. H., and Ferenczi, M. A. (1999) *J. Physiol.*, **520**, 681-696.
80. Bershitsky, S. Y., Ferenczi, M. A., Koubassova, N. A., and Tsaturyan, A. K. (2009) *Front. Biosci.*, **14**, 3188-3213.
81. Fortune, N. S., Geeves, M. A., and Ranatunga, K. W. (1989) *J. Muscle Res. Cell Motil.*, **10**, 113-123.
82. Squire, J. M. (1981) *The Structural Basis of Muscle Contraction*, Plenum, New York.
83. Huxley, H. E. (1968) *J. Mol. Biol.*, **37**, 507-520.
84. Haselgrove, J. C., and Huxley, H. E. (1973) *J. Mol. Biol.*, **77**, 549-568.
85. Matsubara, I., Yagi, N., and Hashizume, H. (1975) *Nature*, **255**, 728-729.
86. Hoskins, B. K., Ashley, C. C., Pelc, R., Rapp, G., and Griffiths, P. J. (1999) *J. Mol. Biol.*, **290**, 77-97.
87. Colson, B. A., Locher, M. R., Bekyarova, T., Patel, J. R., Fitzsimons, D. P., Irving, T. C., and Moss, R. L. (2010) *J. Physiol.*, **588**, 981-993.
88. Malinchik, S., and Yu, L. C. (1995) *Biophys. J.*, **68**, 2023-2031.
89. Wray, J. J. (1987) *Muscle Res. Cell Motil.*, **8**, 62a.
90. Rapp, G., Schrumpf, M., and Wray, J. (1991) *Biophys. J.*, **59**, 35.
91. Bennett, P. M., Tsaturyan, A., and Bershitsky, S. (2002) *J. Microsc.*, **206**, 152-160.
92. Bershitsky, S. Y., Koubassova, N. A., Bennett, P. M., Ferenczi, M. A., Shestakov, D. A., and Tsaturyan, A. K. (2010) *Biophys. J.*, **99**, 1827-1834.
93. Cecchi, G., Griffiths, P., Bagni, M., Ashley, C., and Maeda, Y. (1991) *Biophys. J.*, **59**, 1273-1283.
94. Matsubara, I., Goldman, Y., and Simmons R. M. (1984) *Mol. Biol.*, **173**, 15-33.
95. Fuchs, F., and Martyn, D. A. (2005) *J. Muscle Res. Cell Motil.*, **26**, 199-212.
96. Farman, G. P., Allen, E. J., Gore, D., Irving, T. C., and de Tombe, P. P. (2007) *Biophys. J.*, **92**, L73-75.
97. Huxley, H. E., Stewart, A., Sosa, H., and Irving, T. (1994) *Biophys. J.*, **67**, 2411-2421.
98. Wakabayashi, K., Sugimoto, Y., Tanaka, H., Ueno, Y., Takezawa, Y., and Amemiya, Y. (1994) *Biophys. J.*, **67**, 2422-2435.
99. Bordas, J., Svensson, A., Rothery, M., Lowy, J., Diakun, G. P., and Boesecke, P. (1999) *Biophys. J.*, **77**, 3197-3207.
100. Takezawa, Y., Sugimoto, Y., and Wakabayashi, K. (1998) *Adv. Exp. Med. Biol.*, **453**, 309-316.
101. Tsaturyan, A. K., Koubassova, N., Ferenczi, M. A., Narayanan, T., Roessle, M., and Bershitsky, S. Y. (2005) *Biophys. J.*, **88**, 1902-1910.
102. Linari, M., Dobbie, I., Reconditi, M., Koubassova, N., Irving, M., Piazzesi, G., and Lombardi, V. (1998) *Biophys. J.*, **74**, 2459-2473.
103. Tamura, T., Wakayama, J., Inoue, K., Yagi, N., and Iwamoto, H. (2009) *Biophys. J.*, **96**, 1045-1055.
104. Yagi, N., O'Brien, E. J., and Matsubara, I. (1981) *Biophys. J.*, **33**, 121-138.
105. Squire, J. M., Harford, J. J., Edman, A. C., and Sjostrom, M. J. (1982) *Mol. Biol.*, **155**, 467-494.
106. Huxley, H. E., and Brown, W. (1967) *J. Mol. Biol.*, **30**, 383-434.
107. Martin-Fernandez, M. L., Bordas, J., Diakun, G., Harries, J., Lowy, J., Mant, G. R., Svensson, A., and Towns-Andrews, E. J. (1994) *Muscle Res. Cell Motil.*, **15**, 319-348.
108. Bordas, J., Diakun, G. P., Diaz, F. G., Harries, J. E., Lewis, R. A., Lowy, J., Mant, G. R., Martin-Fernandez, M. L., and Towns-Andrews, E. (1993) *J. Muscle Res. Cell Motil.*, **14**, 311-324.
109. Piazzesi, G., Reconditi, M., Dobbie, I., Linari, M., Boesecke, P., Diat, O., Irving, M., and Lombardi, V. (1999) *J. Physiol.*, **514**, 305-312.
110. Brunello, E., Bianco, P., Piazzesi, G., Linari, M., Reconditi, M., Panine, P., Narayanan, T., Helsby, W. I., Irving, M., and Lombardi, V. (2006) *J. Physiol.*, **577**, 971-984.
111. Linari, M., Piazzesi, G., Dobbie, I., Koubassova, N., Reconditi, M., Narayanan, T., Diat, O., Irving, M., and Lombardi, V. (2000) *Proc. Natl. Acad. Sci. USA*, **97**, 7226-7231.
112. Reconditi, M., Linari, M., Lucii, L., Stewart, A., Sun, Y. B., Boesecke, P., Narayanan, T., Fischetti, R. F., Irving, T.,

Piazzesi, G., Irving, M., and Lombardi, V. (2004) *Nature*, **428**, 578-581.
113. Huxley, H., Reconditi, M., Stewart, A., and Irving, T. (2006) *J. Mol. Biol.*, **363**, 743-761.
114. Huxley, H., Reconditi, M., Stewart, A., and Irving, T. (2006) *J. Mol. Biol.*, **363**, 762-772.
115. Juanhuix, J., Bordas, J., Campmany, J., Svensson, A., Bassford, M. L., and Narayanan, T. (2001) *Biophys. J.*, **80**, 1429-1441.
116. Oshima, K., Takezawa, Y., Sugimoto, Y., Kobayashi, T., Irving, T. C., and Wakabayashi, K. (2007) *J. Mol. Biol.*, **367**, 275-301.
117. Yagi, N., Iwamoto, H., Wakayama, J., and Inoue, K. (2005) *Biophys. J.*, **89**, 1150-1164.
118. Huxley, H. E., Faruqi, A. R., Kress, M., Bordas, J., and Koch, M. H. J. (1982) *J. Mol. Biol.*, **158**, 637-684.
119. Linari, M., Brunello, E., Reconditi, M., Sun, Y. B., Panine, P., Narayanan, T., Piazzesi, G., Lombardi, V., and Irving, M. (2005) *J. Physiol.*, **567**, 459-469.
120. Tsaturyan, A. K., Bershitsky, S. Y., Burns, R., and Ferenczi, M. A. (1999) *Biophys. J.*, **77**, 354-372.
121. Bershitsky, S. Y., and Tsaturyan, A. K. (2002) *J. Physiol.*, **540**, 971-988.
122. Piazzesi, G., Reconditi, M., Koubassova, N., Decostre, V., Linari, M., Lucii, L., and Lombardi, V. (2003) *J. Physiol.*, **549**, 93-106.
123. Irving, M., Piazzesi, G., Lucii, L., Sun, Y. B., Harford, J. J., Dobbie, I. M., Ferenczi, M. A., Reconditi, M., and Lombardi, V. (2000) *Nat. Struct. Biol.*, **6**, 482-485.
124. Bagni, M. A., Colombini, B., Amenitsch, H., Bernstorff, S., Ashley, C. C., Rapp, G., and Griffiths, P. J. (2001) *Biophys. J.*, **80**, 2809-2822.
125. Koubassova, N. A., Bershitsky, S. Y., Ferenczi, M. A., and Tsaturyan, A. K. (2008) *Biophys. J.*, **95**, 2880-2894.
126. Rome, E. (1972) *Cold Spring Harb. Symp. Quant. Biol.*, **37**, 331-339.
127. Haselgrove, J. C. (1975) *J. Mol. Biol.*, **92**, 113-143.
128. Malinchik, S. B., and Lednev, V. V. (1986) *Doklady RAN*, **289**, 1258-1262.
129. Malinchik, S. B., and Lednev, V. V. (1987) *Doklady RAN*, **293**, 238-242.
130. Malinchik, S. B., and Lednev, V. V. (1992) *J. Muscle Res. Cell Motil.*, **13**, 406-419.
131. Hudson, L., Harford, J. J., Denny, R. C., and Squire, J. M. (1997) *J. Struct. Biol.*, **137**, 154-163.
132. Xu, S., Gu, J., Rhodes, T., Belknap, B., Rosenbaum, G., Offer, G., White, H., and Yu, L. (1999) *Biophys. J.*, **77**, 2665-2676.
133. Malinchik, S., Xu, S., and Yu, L. C. (1997) *Biophys. J.*, **73**, 2304-2312.
134. Xu, S., Malinchik, S., Gilroy, D., Kraft, T., Brenner, B., and Yu, L. (1997) *Biophys. J.*, **73**, 2292-2303.
135. Xu, S., Offer, G., Gu, J., White, H., and Yu, L. (2003) *Biochemistry*, **42**, 390-401.
136. Woodhead, J. L., Zhao, F.-Q., Craig, R., Egelman, E. H., Alamo, L., and Padron, R. (2005) *Nature*, **436**, 1195-1199.
137. Urbanke, C., and Wray, J. (2001) *Biochemistry*, **358**, 165-173.
138. Yagi, N. (1992) *J. Muscle Res. Cell Motil.*, **13**, 457-463.
139. Ford, L. E., Huxley, A. F., and Simmons, R. M. (1977) *J. Physiol.*, **269**, 441-515.
140. Yagi, N., Takemori, S., and Watanabe, M. (1993) *J. Mol. Biol.*, **231**, 668-677.
141. Xu, S., Gu, J., Melvin, G., and Yu, L. (2002) *Biophys. J.*, **82**, 2111-2122.
142. Xu, S., Gu, J., Belknap, B., White, H., and Yu, L. C. (2006) *Biophys. J.*, **91**, 3370-3382.
143. Reisler, E., and Egelman, E. H. (2007) *J. Biol. Chem.*, **282**, 36133-36137.
144. Oda, T., Namba, K., and Maeda, Y. (2005) *Biophys. J.*, **88**, 2727-2736.
145. Yagi, N., and Matsubara, I. (1989) *J. Mol. Biol.*, **208**, 359-363.
146. Kraft, T., Mattei, T., Radocaj, A., Piep, B., Nocula, C., Furch, M., and Brenner, B. (2002) *Biophys. J.*, **82**, 2536-2547.
147. Iwamoto, H., Oiwa, K., Kovacs, M., Sellers, J. R., Suzuki, T., Wakayama, J., Tamura, T., Yagi, N., and Fujisawa, T. (2007) *J. Mol. Biol.*, **369**, 249-264.
148. Brenner, B., Yu, L. C., and Podolsky, R. J. (1984) *Biophys. J.*, **46**, 299-306.
149. Brenner, B., and Yu, L. (1993) *Proc. Natl. Acad. Sci. USA*, **90**, 5252-5256.
150. Gu, J., Xu, S., and Yu, L. C. (2002) *Biophys. J.*, **82**, 2123-2133.
151. Huxley, H. E., and Kress, M. (1985) *J. Muscle Res. Cell Motil.*, **6**, 153-161.
152. Yagi, N. (1991) *Adv. Biophys.*, **27**, 35-43.
153. Stehle, R., and Brenner, B. (2000) *Biophys. J.*, **78**, 1458-1473.
154. Yagi, N. (1996) *Acta Cryst. D*, **52**, 1169-1173.
155. Tsaturyan, A. K. (2002) *Acta Crystallogr. A*, **58**, 292-294.
156. Cochran, W., Crick, F. H. C., and Vand, V. (1952) *Acta Crystallogr.*, **5**, 581-586.
157. Yu, L. C. (1989) *Biophys. J.*, **55**, 433-440.
158. Weinstein, B. K. (1963) *X-Ray Diffraction on Chain Molecules* [in Russian], USSR Academy of Sciences, Moscow.
159. Squire, J., and Harford, J. (1984) *Adv. Exp. Med. Biol.*, **170**, 221-236.
160. Harford, J., and Squire, J. (1986) *Biophys. J.*, **50**, 145-155.
161. Al-Khayat, H. A., Hudson, L., Reedy, M. K., Irving, T. C., and Squire, J. M. (2003) *Biophys. J.*, **85**, 1063-1079.
162. Al-Khayat, H. A., and Squire, J. M. (2006) *J. Struct. Biol.*, **155**, 218-229.
163. Xu, S., White, H. D., Offer, G. W., and Yu, L. C. (2009) *Biophys. J.*, **96**, 3673-3681.
164. Rayment, I., Rypniewski, W. R., Schmidt-Base, K., Smith, R., Tomchick, D. R., Benning, M. M., Winkelmann, D. A., Wesenberg, G., and Holden, H. M. (1993) *Science*, **261**, 58-65.
165. Landau, L. D., and Lifshits, E. M. (1987) *Theoretical Physics, Vol. VII. Theory of Elasticity* [in Russian], Nauka, Moscow.
166. Taylor, K. A., Schmitz, H., Reedy, M. C., Goldman, Y. E., Franzini-Armstrong, C., Sasaki, H., Tregear, R. T., Poole, K., Lucaveche, V., Edwards, R. J., Chen, L. F., Winkler, H., and Reedy, M. K. (1999) *Cell*, **99**, 421-431.
167. Wu, S., Liu, J., Reedy, M. C., Tregear, R. T., Winkler, H., Franzini-Armstrong, C., Sasaki, H., Lucaveche, C., Goldman, Y. E., Reedy, M. K., and Taylor, K. A. (2010) *PLoS One*, **9**, e12643.2010.
168. Holmes, K. C., Tregear, R. T., and Barrington Leigh, J. (1980) *Proc. R. Soc. B.*, **207**, 13-33.
169. Sqiure, J. M., and Harford, J. J. (1988) *J. Muscle Res. Cell Motil.*, **9**, 344-358.
170. Holmes, K. C., Angert, I., Kull, F. J., Jahn, W., and Schroeder, R. R. (2003) *Nature*, **425**, 423-427.
171. Koubassova, N. A., and Tsaturyan, A. K. (2002) *Biophys. J.*, **83**, 1082-1097.